

**Title: Smad4 modulates glycolysis and OXPHOS via interactions with
PKM2 and ATPIF1 in diabetic nephropathy**

Authors: Jinhua Li^{1,2,3,4,5,6*#§}, Yu Bo Yang Sun^{3§}, Weiyi Chen⁷, Jinjin Fan^{5,6}, Songhui Li^{8,9}, Xinli Qu³, Qikang Chen¹, Riling Chen¹, Dajian Zhu¹, Jinfeng Zhang¹, Honggang Chi², Simon Crawford¹⁰, Viola Oorschot¹⁰, Victor G. Puelles^{11,12}, Peter G Kerr¹², Yi Ren¹³, Susan K. Nilsson^{8,9}, Mark Christian¹⁴, Huanwen Tang¹⁵, Wei Chen^{5,6}, John F. Bertram³, David J. Nikolic-Paterson¹², Xueqing Yu^{1,6, 16*}

Affiliations:

¹ Shunde Women and Children Hospital, Guangdong Medical University, Shunde, Guangdong, 528300, China;

²The Second Clinical College, Guangdong Medical University, Dongguan, Guangdong, 528399, China;

³Department of Anatomy and Developmental Biology, Monash Biomedicine Discovery Institute, Monash University, Clayton, Victoria, 3800, Australia;

⁴Department of Physiology, Monash Biomedicine Discovery Institute, Monash University, Clayton, Victoria, 3800, Australia;

⁵Department of Nephrology, the First Affiliated Hospital, Sun Yat-sen University, 58th, Zhongshan Road II, Guangzhou, 510080, China;

⁶Key Laboratory of Nephrology, National Health Commission and Guangdong Province, Guangzhou, 510080, China;

⁷Department of Biochemistry and Molecular Biology, Monash University, Clayton, Victoria, 3800, Australia;

⁸Biomedical Manufacturing Commonwealth Scientific and Industrial Research Organisation (CSIRO), Melbourne, Victoria, 3168, Australia;

⁹Australian Regenerative Medicine Institute, Monash University, Clayton, Victoria, 3800, Australia;

¹⁰Monash Ramaciotti Cryo EM platform, Monash Biomedicine Discovery Institute,

¹¹Nephrology and Immunology, RWTH Aachen University, Aachen 52074, Germany;

¹²Department of Nephrology, Monash Health and Monash University Department of Medicine, Clayton, Victoria, 3168, Australia;

¹³Department of Biomedical Sciences, Florida State University College of Medicine, Tallahassee, FL, 32306, USA;

¹⁴Division of Biomedical Sciences, Warwick Medical School, University of Warwick, Coventry, CV4 7AL, UK;

¹⁵Department of Preventive Medicine, Dongguan Key Laboratory of Environmental Medicine, School of Public Health, Guangdong Medical University, Dongguan, 523808, Guangdong, China

¹⁶Guangdong Academy of Medical Science, Guangdong Provincial People's Hospital, Guangzhou, 510080, China

[§]Both authors contributed equally to this work.

Running Head: Smad4 in diabetic nephropathy

Counting Characters: 56,902

* Corresponding Authors:

Jinhua Li, MBBS, PhD

Department of Physiology

Monash University, Clayton, Victoria 3800, Australia

E-mail: jinhua.li@monash.edu

Phone: 61 3 9902 9103

Xueqing Yu, MD, PhD

Guangdong Academy of Medical Science, Guangdong Provincial People's Hospital,

Guangzhou, 510080, China

E-mail: yuxq@mail.sysu.edu.cn

Phone: 86 20 83827812-21168

Fax: 86 20 83827712

Abstract

Diabetic nephropathy (DN) is the leading cause of end-stage kidney disease. TGF- β 1/Smad3 signalling plays a major pathological role in DN; however, the contribution of Smad4 has not been examined. Knock-down of Smad4 expression in the kidney using an anti-*Smad4* locked nucleic acid halted progressive podocyte damage and glomerulosclerosis in mouse type 2 DN, suggesting a pathogenic role of Smad4 in podocytes. We identified up-regulation of Smad4 in podocytes in human and mouse DN. Next, conditional *Smad4* deletion in podocytes was shown to protect mice from type 2 DN independent of obesity. Mechanistically, hyperglycaemia induces Smad4 localisation to mitochondria in podocytes resulting in reduced glycolysis and oxidative phosphorylation, and increased production of reactive oxygen species. This operates, in part, via direct binding of Smad4 to the glycolytic enzyme PKM2 to reduce the active tetrameric form of PKM2. In addition, Smad4 interacts with ATPIF1, causing a reduction in ATPIF1 degradation. In conclusion, we have identified a novel mitochondrial-based mechanism by which Smad4 causes diabetic podocyte injury.

Keywords: ATPIF1, PKM2, podocyte, Smad4, type 2 diabetic nephropathy.

Introduction

Type 2 diabetes is the most common cause of end-stage renal disease (ESRD) in developed countries. Current therapies rely upon treatment of hyperglycaemia and control of hypertension, focusing on inhibition of the renin-angiotensin-aldosterone system (RAAS) [1]. Despite attempts at optimal blood glucose and blood pressure control, diabetic nephropathy (DN) develops in many patients [2, 3], indicating that additional approaches are needed to halt the development and progression of DN.

TGF- β 1 regulates a diverse range of cellular responses [4], including proliferation, wound healing, differentiation, fibrosis, apoptosis and metabolism. Studies in human and experimental DN have identified a key role for TGF- β 1 in the development and progression of DN [5]. However, systemic targeting of TGF- β 1 carries significant risks as demonstrated by the severe organ inflammation and early lethality seen in mice lacking *Tgfb1* [6], *Tgfb1* [7], or lacking *Tgfb2* in T cells [8]. Therefore, approaches are needed to target factors downstream of TGF- β 1 and its receptor to suppress disease development.

TGF- β 1 exerts its major biological effects through its cell surface receptors; TGF- β RI and TGF- β RII [4]. Upon TGF- β 1 binding, the TGF- β RI phosphorylates Smad2 and Smad3 which then oligomerize with Smad4 to form a complex that translocates into the nucleus. Smad3 and/or Smad4 can directly bind to DNA sequences or cofactors to regulate transcription of their target genes [4]. Global deletion of *Smad2* or *Smad4* is lethal, whereas *Smad3* deficient mice are viable [9], leading to a major focus on TGF- β 1/Smad3 signalling. Mice lacking *Smad3* are resistant in many models of tissue fibrosis [10]. In particular, *Smad3* deficient mice are protected from albuminuria and renal fibrosis in type 1 DN [11], and are resistant to high fat diet (HFD) induced obesity, insulin resistance and diabetes [12, 13]. In addition, *Smad3* deficiency protects mice from HFD-induced kidney disease [14]. By contrast, little is

known about Smad4 in diabetes or DN. Blockade of Smad4 in pancreatic beta cells attenuated HFD-induced glucose intolerance, but not insulin resistance [15], while Smad4 protein levels in skeletal muscle are up-regulated in the obese subjects compared to the lean subjects [16]. Of note, activation of AMP-activated protein kinase (AMPK) inhibits nuclear translocation of Smad4, reduces mesangial matrix accumulation and early DN [17]. In addition, studies in colon cancer cells show that *Smad4* deficiency increases aerobic glycolysis and enhances cell migration [18]. Taken together, these lines of evidence suggest that Smad4 may play a distinct role in metabolism which could be relevant to obesity and type 2 diabetes. Therefore, the aim of the current study was to determine whether Smad4 plays a pathologic role in type 2 DN.

We investigated Smad4 function in kidney disease in a well validated mouse model of accelerated type 2 diabetes which employs HFD and a single low dose streptozotocin (STZ) injection [19-28]. The HFD/STZ model was performed in hypertensive *eNOS* deficient mice which have increased susceptibility to diabetic kidney disease [29-31]. Knock-down of Smad4 expression in the kidney halted the progression of DN. Furthermore, conditional *Smad4* deletion in podocytes was sufficient to protect against DN, without affecting obesity. Under diabetic conditions, Smad4 was present in podocyte mitochondria in association with reduced glycolysis and oxidative phosphorylation (OXPHOS), and increased production of reactive oxygen species. We show that Smad4 interacts directly with the rate-limiting glycolytic enzyme PKM2 and with ATPase Inhibitory Factor 1 (ATPIF1) to regulate glycolysis and OXPHOS in podocytes, respectively. In summary, our study uncovers both a pathologic role and a novel mechanism of action by which Smad4 in podocytes promotes kidney disease in type 2 diabetes.

Results

Knock-down of Smad4 in the kidney improves renal function and halts progression of type 2 DN

To investigate the role of Smad4 in the progression of type 2 DN, we used systemic administration of a Locked Nucleic Acid (LNA) to knock-down Smad4 mRNA and protein expression in the kidney. LNA are nucleic acid analogues in which the ribose ring is “locked” by a methylene bridge [32,33], resulting in increased target specificity and resistance to both exonucleases and endonucleases, giving excellent stability *in vivo*[34-36]. In particular, LNA anti-sense oligonucleotides exhibit preferential uptake by the kidney[37, 38].

First, we validated efficient Smad4 knock-down in cultured podocytes 4 days after the addition of Smad4 LNA, while control LNA did not affect Smad4 expression (**Fig. 1A**). Next, we sought to knock-down Smad4 in type 2 diabetes with established kidney disease. In this model, hypertensive *eNOS*^{-/-} mice on the C57BL/6J background are placed on a high fat diet (HFD) for 30 weeks with a single STZ injection on week 8 to further increase blood glucose levels to diabetic state while remaining hyperinsulinaemia, a characteristic of type 2 diabetes [19-31]. This regimen results in hyperglycaemia, hyperinsulinaemia, albuminuria, glomerulosclerosis and reduced kidney function (**Suppl. Fig 1**). Groups of 8 mice were treated with 10mg/kg Smad4 LNA or control LNA (CTL LNA) by once weekly intraperitoneal injection from week 24 until being killed at week 30 (**Fig. 1B**). Smad4 LNA efficiently down-regulated Smad4 protein levels in the kidney, without affecting protein levels of Smad3 or the glycolysis enzyme, PKM2 (**Fig. 1C&D**). In addition, we demonstrated efficient knock-down of Smad4 in podocytes isolated from these mice (**Fig. 1E**). By contrast, Smad4 expression in liver, lung and spleen was unaffected by Smad4 LNA treatment (**Fig**

1F-H). Body weight, glucose intolerance and hyperglycemia were equivalent in the LNA treated groups as shown by HbA1c levels (**Fig. 1I & Suppl. Fig 2**). CTL LNA treated mice exhibited substantial podocyte damage at week 30 as shown by a reduction in the number of podocytes (defined by p57 immunostaining) and by a reduction in the area of staining for the podocyte marker, synaptopodin (**Fig 1J&K and Suppl. Fig 3A-C**). Smad4 LNA treatment also significantly reduced the severity of glomerulosclerosis compared to CTL LNA treatment as illustrated by PAS staining and quantified using collagen IV deposition (**Fig. 1L-O and Suppl. Fig 3D-F**). In addition, Smad4 LNA treatment significantly reduced albuminuria (urine albumin to creatinine ratio) and improved renal function (serum cystatin C levels) in established DN compared to CTL LNA (**Fig. 1P&Q**). Taken together, these data demonstrate that administration of Smad4 LNA can selectively target Smad4 expression in the kidney and halt the progression of established DN, independent of the diabetic state.

Upregulation of Smad4 in podocytes in type 2 DN

The protective effects of Smad4 LNA in type 2 DN could be accounted for, at least in part, by protecting podocytes from injury. Therefore, we examined podocyte Smad4 expression in human and mouse DN. Confocal microscopy showed Smad4 staining in glomerular cells, including WT1+ podocytes, in normal human kidney, with relatively little co-localisation of Smad4 with the mitochondrial marker Tom20 (**Fig 2A, C and E**). Note that the WT1 antibody used recognizes an isoform of WT1 present in the cytoplasm, not in the nucleus, of podocytes [39, 40]. A marked increase in Smad4 expression was evident in glomerular podocytes in diabetic nephropathy, with co-localisation of Smad4 and Tom20 evident in some cells (**Fig 2B, D and F**).

Smad4 staining is also evident in some podocytes in normal mouse kidney, with little co-localisation of Smad4 with Tom20 (**Fig 2G, I and K**). However, diabetic kidneys exhibited up-regulation of Smad4 in glomeruli, with some Smad4 protein clearly co-localising with Tom20 in some glomerular cells, including podocyte-like cells (**Fig 2H, J and L**). Up-regulation of Smad4 in podocytes is a relatively early event in mouse DN, with Western blotting of isolated podocytes showing increased Smad4 protein levels after 4 weeks of diabetes (**Fig 2M-O**). These findings suggest a potential role for Smad4 in podocyte metabolism.

Smad4 deficiency in podocytes preserves renal function and protects mice from glomerulosclerosis in type 2 DN

To specifically address the question of whether Smad4 affects podocyte function in type 2 DN, we generated *eNOS*^{-/-} mice with *Smad4* deletion in podocytes (*eNOS*^{-/-};*PodCre-Smad4*^{fllox/fllox} mice) on the C57BL/6J background. Mice lacking Smad4 in podocytes have a normal phenotype. We then induced type 2 DN using the 30 week HFD/STZ model in *eNOS*^{-/-};*PodCre-Smad4*^{-/-} and *eNOS*^{-/-};*PodCre* littermate controls. Both mouse genotypes developed equivalent obesity, elevated blood glucose and HbA1c levels, hyperinsulinaemia and glucose intolerance (**Suppl Fig 4A-F**). To validate conditional *Smad4* deletion, podocytes were isolated from diabetic and non-diabetic control kidneys by flow cytometry. Western blot analysis confirmed efficient *Smad4* deletion in podocytes from *eNOS*^{-/-};*PodCre-Smad4*^{-/-} mice (**Fig 3A**). Compared to control diabetic mice, diabetic *eNOS*^{-/-};*PodCre-Smad4*^{-/-} mice were substantially protection against podocyte damage in terms of loss of p57+ podocytes and down-regulation of the podocyte specific protein, nephrin (**Fig 3B-D**). Control diabetic mice exhibited glomerular hypertrophy, mesangial matrix expansion (PAS staining), glomerulosclerosis (increased glomerular collagen IV deposition), reduced renal function

(increased serum cystatin C) and albuminuria (increased urine albumin/creatinine ratio) (**Fig 3E-I**). By comparison, diabetic *eNOS^{-/-};PodCre-Smad4^{-/-}* mice showed marked protection against mesangial matrix expansion and glomerulosclerosis, although glomerular hypertrophy was still evident (**Fig 3E-G**). In addition, diabetic *eNOS^{-/-};PodCre-Smad4^{-/-}* mice showed improved renal function and reduced albuminuria (**Fig 3H&I**). Thus, Smad4 deficiency in podocytes preserved renal function and protected mice from kidney injury despite unaltered diabetes and obesity (**Suppl Fig. 4**).

Smad4 deficiency in podocytes promotes glycolysis and OXPHOS activity under high glucose conditions

Ozawa et al [41] demonstrated that glycolysis is a major contributor to intracellular ATP production in podocytes and that phosphofructokinase, a rate limiting enzyme for glycolysis, is expressed in podocyte foot processes. This suggests an important role for glycolysis in normal podocyte function, leading us to investigate whether the protective effects of *Smad4* deletion in podocytes are related to glycolysis.

The Seahorse Glycolysis Stress Test demonstrated that glycolysis, glycolytic capacity, glycolytic reserve and non-glycolytic acidification were increased in *Smad4^{-/-}* compared to wild type podocytes under both normal (NG, 1g/L D-glucose) and high glucose (HG, 4.5g/L D-glucose) conditions (**Fig 4A&B**). The Seahorse Cell Mito Stress Test demonstrated that *Smad4* deficiency increased basal, maximal and ATP-linked respiration, but not proton leak, in podocytes under both normal and high glucose conditions (**Fig 4C&D**), indicating that Smad4 deficiency increases OXPHOS activity. Electron microscopy showed that *Smad4* deficiency did not alter mitochondrial morphology (**Fig 4E&F**). *Smad4* deficiency in cultured

podocytes did not alter mitochondrial copy number (**Fig 4G**), or change protein levels of three rate-limiting glycolytic enzymes or PGC-1 α , the mitochondrial biogenesis marker (**Fig 4H**). Compared to wild type podocytes, *Smad4* deficient podocytes have a greater capacity for lactate production (**Fig 4I&J**), and have reduced reactive oxygen species (ROS) production under both normal and high glucose conditions (**Fig 4K-M**). In addition, *Smad4* deficiency prevented high glucose-induced up-regulation of NOX4 expression and down-regulation of synaptopodin (**Fig 4N**). NOX4 is the main source of ROS in the kidney and *Nox4* is increased in DN and in podocytes in response to high glucose [42-44]. Podocyte-specific *Nox4* deletion protects mice from diabetic nephropathy and this protection is associated with reduced renal ROS production [44]. Our studies demonstrated that *Smad4* deletion promotes glycolysis, modulates OXPHOS activity, reduces NOX4 expression and ROS production, and prevents high glucose-induced injury in podocytes.

Smad4 modulates glycolysis in podocytes through interaction with PKM2

Next, we investigated the mechanism by which *Smad4* regulates glycolysis in podocytes. Protein levels of the glycolytic enzyme, PKM2, were increased in the kidney of mouse type 2 DN compared to age-matched, non-diabetic controls (**Fig 5A&B**). In isolated podocytes, immunoprecipitation studies identified binding between *Smad4* and PKM2 in non-diabetic cells, and this interaction was increased in podocytes from diabetic mice (**Fig 5C and D**). A time-course study showed that lactate production falls as the interaction between *Smad4* and PKM2 increases during the culture of podocytes under high glucose conditions (**Fig 5E**). Podocytes isolated from age-matched *PodCre-Smad4*^{-/-} mice did not show a difference in PKM2 expression (**Fig 4G**). However, compared to wild type podocytes, cultured *Smad4*^{-/-} podocytes showed increased PKM2 activity under both normal and high glucose conditions

(**Fig 5F**), suggesting that Smad4 may modulate PKM2 activity. The active form of PKM2 has a tetramer structure, whereas dimer and monomer forms are inactive [45]. Cross-linking studies showed that high glucose stimulation of podocytes caused a reduction in the active form of PKM2 (tetramer), while Smad4 deficient podocytes exhibited significantly greater levels of the PKM2 tetramer under both normal and high glucose conditions (**Fig 5G and H**). This led us to hypothesize that Smad4 may interact with PKM2 to inhibit the formation of PKM2 tetramer.

To further investigate the Smad4/PKM2 interaction, 293T cells were co-transfected with Flag-tagged PKM2 and HA-tagged Smad4 expression plasmids and cross-linking studies performed. Decreasing HA-Smad4 expression (upper panel) resulted in a decrease in the interaction between HA-Smad4 and Flag-PKM2 (middle panel) and the increase in the tetramer form of PKM2 and the ratio of the tetramer to dimer + monomer forms (lower panel) (**Fig 5I**). This findings provides direct evidence that Smad4 interacts with PKM2 to inhibit PKM2 tetramer formation.

Canonical TGF- β 1/Smad4 signalling involves Smad4 translocation to the nucleus to regulate gene transcription [4]. Indeed, mutations of the key amino acids (R100T and L43S) that facilitate Smad4 nuclear translocation prevent transcription of the Smad-binding element (SBE) [46]. If Smad4 modulation of podocyte metabolism operates via a non-canonical pathway, then it should be unaffected by blocking Smad4 nuclear localisation. To address this question, *Smad4*^{-/-} podocytes were transduced with retroviral vectors expressing wild type (Smad4^{WT}) or the mutants, Smad4^{R100T} or Smad4^{L43S}, which prevent Smad4 entry into the nucleus [46]. First, we confirmed that Smad4^{R100T} and Smad4^{L43S} expressing cells had a

greatly diminished response to TGF- β 1 stimulation in the SBE4-luciferase assay compared to Smad4^{WT} cells (**Fig 5J**), a response that depends upon Smad4 nuclear localisation [46]. Next, we used immunoprecipitation to show that Smad4^{R100T}/PKM2 and Smad4^{L43S}/PKM2 interactions are comparable to that of Smad4^{WT}/PKM2 (**Fig 5K**). In addition, cells transduced with Smad4^{R100T} or Smad4^{L43S} were comparable to Smad4^{WT} transduced cells in terms of: PKM2 tetramer formation (**Fig 5L**), lactate and ROS production (**Fig 5M&N**), synaptopodin expression (**Fig 5O**) and NOX4 expression (**Fig 5P**). These data show that Smad4 regulation of glycolysis is independent of a Smad4 nuclear function.

Quantitative proteomic analysis identifies downregulation of ATP1F1 in Smad4 deficient podocytes

Smad4 deficiency increased OXPHOS activity in podocytes, but did not alter mitochondrial morphology (**Fig 4E&F**). To investigate molecular mechanism(s) by which Smad4 regulates mitochondrial OXPHOS activity, we performed Mass Spectrometry (MS)-based quantitative proteomic analysis in mouse podocytes. First, we treated *Smad4* deficient and WT mouse podocytes with normal or high glucose. Then, the protein was digested, labeled with TMT reagents and analyzed by MS for proteome quantification. We identified 5228 protein groups in the four experimental groups with three biological replicates. We defined significantly different ($p < 0.05$ by two tailed t-test) proteins and used a criterion of 1.3-fold change or greater between two groups as differential protein candidates. Subsequently, the numbers of downregulated and upregulated proteins in the four groups were identified (**Fig 6A & Suppl Table 1**). Bioinformatics enrichment analysis with gene ontology (GO) and Kyoto Encyclopedia of Genes and Genomes (KEGG) databases by the ClueGO tool [47] revealed that metabolic process, binding and catalytic activity are the most highly enriched pathways involving Smad4 (**Fig 6B & Suppl. Fig 5**). MS revealed that *Smad4* deficiency markedly

reduces protein levels of ATPase Inhibitory Factor 1 (ATPIF1), the inhibitor of ATP synthase and the regulator of the activity of OXPHOS in mammalian tissues [48, 49], compared to WT podocytes under both normal and high glucose conditions (**Fig 6C**). MS also identified downregulation of Mitochondrial Pyruvate Carrier 1 (MPC1), which controls the influx of pyruvate into mitochondria for OXPHOS, and proteins involved in the Mitochondrial Respiratory Chain, such as Ndufs4, Ndubf10, Uqcrcb, Cox7a21 and Cox5a (**Fig 6C**). The increase in ATP synthase activity caused by severe inhibition of ATPIF1 and the limitation of pyruvate influx into mitochondria attributable to downregulation of MPC1, prompted us to investigate whether *Smad4* deficiency may increase mitochondrial OXPHOS efficiency and therefore decrease mitochondrial ROS production and ultimately contribute to the protection of *Smad4* deficient podocytes from high glucose-induced injury.

Smad4 binds to ATPIF1 and reduces ATPIF1 degradation

We investigated the mechanism by which *Smad4* deficiency in podocytes caused down-regulation of ATPIF1. Western blotting confirmed a significant reduction of ATPIF1 and MPC1 protein levels in *Smad4* deficient podocytes under both normal and high glucose conditions (**Fig 7A**). *Smad4* deficiency significantly protected podocytes from high glucose-induced loss of ATP production (**Fig 7B**), suggesting that *Smad4* deficiency increases the activity of ATP synthase through down-regulation of ATPIF1.

To investigate how *Smad4* deletion alters ATPIF1 expression, we examined both mRNA and protein stability. *Smad4* deficiency did not change ATPIF1 mRNA levels in mouse podocytes (**Fig 7C**). Next, we analysed whether *Smad4* affects ATPIF1 mRNA half-life using Actinomycin-D to shut-off transcription. Similar decay curves were seen for ATPIF1 mRNA

in both *Smad4* deficient and wild type cells (**Fig 7D**), suggesting that Smad4 regulates ATPIF1 at the posttranscriptional level. We examined ATPIF1 protein stability in mouse podocytes finding a very rapid accumulation of ATPIF1 protein in response to o-phenanthroline (O-Phe), an inhibitor of mitochondrial proteases (**Fig 7E**) [49]. After removal of O-phe and addition of cycloheximide to stop *de novo* protein synthesis, cells were followed for varying periods of time. Western blot decay curves demonstrated that *Smad4* deficiency decreased the half-life of ATPIF1 protein (**Fig 7E&F**). Immunoprecipitation showed an interaction between Smad4 and ATPIF1 which was increased in podocytes isolated from type 2 DN compared to age-matched mouse kidneys (**Fig 5C&D**).

To investigate whether Smad4 is required for ATPIF1 protein stability, we employed titratable, doxycycline (dox)-inducible sgRNA cassette/cas9 system to delete the *Smad4* gene in a mouse podocyte cell line. Immunoprecipitation studies showed a dose-dependent knock-down of Smad4 with increasing dox concentration. This caused a reduction in ATPIF1 protein levels in association with a reduction in Smad4 binding to ATPIF1 (**Fig 7G**), suggesting that the interaction of Smad4 with ATPIF1 may protect ATPIF1 from degradation. Seahorse analysis demonstrated a dose-dependent increase in basal respiration, maximal respiration and ATP-linked respiration with down-regulation of Smad4 and ATPIF1 (**Fig 7H-J**), suggesting that Smad4 regulates mitochondrial OXPHOS activity through ATPIF1. To demonstrate that this effect was independent of Smad4 nuclear localization, we used retroviral-mediated Smad4^{WT}, Smad4^{R100T} and Smad4^{L43S} expression in *Smad4* deficient podocytes as previously above. Immunoprecipitation studies showed that the Smad4^{R100T}/ATPIF1 and Smad4^{L43S}/ATPIF1 interactions are comparable to the Smad4^{WT}/ATPIF1 interaction (**Fig 7K**). There is no significant difference in basal, maximal and ATP-linked respiration, proton leak, or ATP levels between podocytes expressing

Smad4^{WT}, Smad4^{R100T} or Smad4^{L43S} (**Fig 7L-N**). Taken together, our data suggests that Smad4 may interact with ATP1F1 to modulate OXPHOS activity. The decreased expression level of MPC1 (**Fig 7A**) further suggests that Smad4 deficiency may increase OXPHOS efficiency through limitation of pyruvate influx into mitochondria and augmentation of OXPHOS activity in mouse podocytes.

Discussion

The present study demonstrates that *Smad4* deficiency protects podocytes from high glucose-induced injury through enhanced glycolysis and maintenance of mitochondrial OXPHOS, which consequently decreases NOX4 expression and ROS production. This is attributed to a non-canonical action of *Smad4* in regulating glycolysis and OXPHOS via direct interactions with the rate-limiting glycolytic enzyme, PKM2, and with ATP1F1. Conditional *Smad4* deletion in podocytes protects against the development of DN, while Smad4 LNA halted the progression of established DN, identifying Smad4 as a therapeutic target in DN.

Podocyte foot processes form slit diaphragms which are part of the glomerular filtration barrier that limits albumin filtration into the urinary space. Movement of foot processes in response to environmental changes requires the redistribution of actin filaments which is dependent upon phosphorylation-mediated signaling. This requires high levels of ATP to maintain normal podocyte structure and function [41, 50]. Mitochondria and glycolysis maintain energy homeostasis in podocytes [41, 51], with glycolysis responsible for the intracellular ATP distribution in the cortical area of podocytes [41]. Mitochondrial dysfunction with insufficient ATP production may contribute to the development of DN [52-54]. We identified direct interactions between Smad4 and PKM2 and ATP1F1; key enzymes

in glycolysis and OXPHOS. These interactions were associated with reduced glycolysis and lactate production in podocytes under high glucose conditions, indicating that podocyte glycolysis is diminished in DN. The enhancement of glycolysis in *Smad4* deficient podocytes may compensate for the loss of ATP due to mitochondrial injury, thus preventing podocyte damage and podocyte loss in the diabetic milieu.

The mitochondrial H⁺-ATP synthase is the master of OXPHOS that catalyzes the synthesis of ATP using the proton gradient generated by the respiratory chain [55]. ATP1F1 is the biological inhibitor of the H⁺-ATP synthase [56, 57]. Overexpression of ATP1F1 leads to the inhibition of the ATP synthesis and the switch to an increased aerobic glycolysis in cancer cells [58]. By contrast, inhibition of ATP1F1 can ameliorate severe electron transport chain dysfunction due to reversal of the F1-F0 ATP synthase, thus maintaining mitochondrial membrane potential [59]. In our study, *Smad4* deficiency increased pyruvate production through enhancement of glycolysis, but the reduction of MPC1 decreases the pyruvate influx into mitochondria for OXPHOS, thus reducing the ROS production. On the other hand, the reduced levels of ATP1F1 seen with *Smad4* deletion increased activity of the H⁺-ATP synthase, resulting in the augmentation of OXPHOS efficiency and an increase in ATP production. Thus, *Smad4* deficiency protects podocytes from high glucose-induced injury through this fine tuning of mitochondrial activity by positive and negative regulators.

Hyperglycaemia plays an essential role in the pathogenesis of DN. Increased intracellular glucose results in accumulation of toxic glucose metabolites which exacerbates the development of DN [60, 61]. Podocyte injury and loss are early pathological changes in the pathogenesis of DN [62, 63]. Qi et al [64] found that enzymes in the glycolytic and

mitochondrial pathways are increased in individuals with long duration of diabetes but are protected from DN. They further demonstrated that TEPP-46, a PKM2 activator, protected mice against DN by increasing glucose metabolic flux, inhibiting the production of toxic glucose metabolites and inducing mitochondrial biogenesis to restore mitochondrial function. We showed that *Smad4* deficiency in podocytes enhances glycolysis and lactate production, decreases NOX4 expression and ROS production, and protects against high glucose-induced injury *in vitro*. Importantly, mice with *Smad4* deletion in podocytes exhibited significant protection against podocyte damage and the development of glomerulosclerosis, albuminuria and impaired renal function despite unaltered obesity and diabetes. These *in vivo* findings further support the hypothesis that an increase in glycolysis and lactic acid production may decrease intracellular free glucose and toxic glucose metabolites, thus reducing high glucose-induced injury and providing salutary effects in DN.

In canonical TGF- β /Smad signalling, Smad4 enters the nucleus as part of a complex with phosphorylated Smad2 and Smad3 which binds to promoter regions of target genes to regulate transcription [4]. However, recent studies demonstrate that Smad4 may directly translocate to mitochondria and interact with the mitochondrial protein cytochrome c oxidase II to promote apoptosis [65]. CHCHD2, a mitochondrial protein, interacts with Smad4 to repress TGF- β signalling in human induced pluripotent stem cells [66]. Our study demonstrated that Smad4 expression is increased in the podocyte cytoplasm in both human and mouse DN. The interactions between Smad4 and the rate-limiting glycolytic enzyme PKM2, and between Smad4 and ATP1F1, were increased in mice with DN. The interaction between Smad4 and PKM2 reduced the tetramer form of PKM2 and PKM2 activity, thus reducing glycolysis and lactate production under high glucose conditions in podocytes. The Smad4/ATP1F1 interaction protects ATP1F1 from degradation. Notably, using Smad4 R100T

and L43S mutations, we identified that nuclear localisation was not required for Smad4 interactions with PKM2 and ATP1F1 in mitochondria, or for Smad4 modulation of glycolysis and ATP production. Thus, cytoplasmic Smad4 regulates glycolysis and OXPHOS via a novel, non-canonical pathway.

LNA technology is currently being used in clinical trials [67]. The substantial renal accumulation of LNA at pharmacologically active levels makes it a feasible strategy for the treatment of kidney disease [37, 38]. Delivery of the Smad4 LNA reagent significantly decreased Smad4 expression in kidneys, but not in the liver, spleen or lung. This selective effect upon the kidney in experimental DN was supported by the lack of effect of Smad4 LNA on body weight, hyperglycaemia, hyperinsulinaemia and impaired glucose tolerance. While the findings of Smad4 LNA treatment are consistent with the protective effects of Smad4 deletion in podocytes, clearly the beneficial effects of this treatment could also involve actions on other cell types.

There are a number of limitations in these studies. The overall effects of *Smad4* deletion in podocytes reported here may not be solely attributed to the changes observed in glycolysis and mitochondrial OXPHOS. It is feasible that other mechanisms such as fatty acid oxidation may have influenced the overall phenotype in Smad4 deficient podocytes. In addition, Smad4 shuttles to the nucleus as a transcription factor to regulate gene transcription which could also have contributed to the effects seen with *Smad4* deletion [46]. How signalling pathway(s) induce interactions between Smad4 and rate-limiting glycolytic enzymes PKM2 and ATP1F1 were not investigated. Finally, mitochondrial measures such as citrate synthase activity were outside of the scope of this manuscript but certainly warrant further investigation.

In conclusion, these results provide new insights into the role of Smad4 in the pathogenesis of diabetic nephropathy. Specifically, we describe a previously unrecognised action of cytoplasmic Smad4 in the regulation of glycolysis and OXPHOS. These observations suggest that pharmacological approaches to inhibit Smad4 activity in the kidney could represent a therapeutic strategy for the treatment of type 2 DN.

Methods

Experimental animals and diets

Breeding pairs of *eNOS*^{-/-} mice, Smad4^{fl/fl} mice, tamoxifen-inducible Tg(CAG-cre/Esrr1)5Amc/J mice (ER-Cre), and 2.5P-Cre;Tg(NPHS2-cre)1Lbh mice were purchased from Jackson Laboratories (Bar Harbor, ME) and maintained at Monash Animal Services. Mice were fed a ND or a HFD (Specialty Feeds, Glen Forrest, WA, Australia) for 8 weeks first, followed by a single low dose of STZ injection (Sigma, St Louis, MO) and continued with HFD treatment for another 16 weeks. ND provided 1.68MJ/kg of energy from lipid (20% protein and 4.8% total fat). HFD provided 8.17MJ/kg of energy from lipid (22.6% protein and 23.5% total fat). In all experimental procedures, mice were housed in a controlled environment and food and water were available *ad libitum*. Body weights were measured weekly. To delete Smad4 gene, tamoxifen (20mg/kg) was given to *eNOS*^{-/-}:*ErCre-Smad4*^{fl/fl} mice through intraperitoneal injection for 5 days consecutively. All experiments were approved by the Monash University Animal Ethics Committee and adhered to the Australian Code of Practice for the Care and Use of Animals for Scientific Purposes.

Human Renal Biopsy Specimens

Studies using human tissue were approved by the Human Ethics Committee of Monash Medical Centre, and written informed consent was obtained from the patients. Paraffin sections of renal biopsies, excess to that required for diagnosis, were examined in four cases of diabetic nephropathy. Normal kidney tissue was obtained from the noninvolved pole of nephrectomies performed as the result of renal carcinoma.

LNA intervention study

Smad4 LNA and CTL LNA were designed by and purchased from Exiqon, Denmark. Smad4 LNA: 5'-TTGATGCGCGATTACT-3'; negative control LNA (CTL LNA): 5'-AACACGTCTATACGC-3'. Smad4 LNA potency was confirmed in cultured differentiated podocytes and 8 weeks old normal adult C57BL/6 J mice. Smad4 LNA and CTL LNA were dissolved in 1X PBS and directly added to cultured podocytes at final concentration of 1, 5 and 10 μ M respectively. Cultured medium were changed and Smad4 LNA or CTL LNA was added every day. Cells were harvested for protein analysis 4 days after the initial treatment. A preliminary experiment was performed to determine the effective dose range of Smad4 LNA in type 2 DN. A dose curve of Smad4 LNA or CTL LNA ranging from 5 to 20 mg/kg was administered to normal 8 weeks old C57BL/6J mice (7 groups/ n = 2 mice each). Mice were killed after Smad4 LNA or CTL LNA administration; kidney tissues were collected to detect expression levels of Smad4 by Western blotting. Based on the results from this study, 10mg/kg Smad4 LNA or CTL LNA dissolved in 1X PBS was intraperitoneally injected into *eNOS* deficient type 2 DN mice once a week for 6 weeks. Mice were killed. Blood, urine, organs/tissues were collected for further analysis. No obvious side effects were observed during the experiments and in the organs/tissues examined.

Lactate levels in cell culture supernatant

The concentration of lactate in podocytes, the end product of glycolysis, was determined using the lactate colorimetric assay kit (Abcam, Cambridge, United Kingdom). The OD was measured at 450 nm and the standard curve plot (nmol/well vs. OD 450 nm) was then generated. Finally, the lactate concentrations were determined as follows: $C = La/10^6$ cells in a period time (mmol/l/ 10^6 cells).

Microalbuminuria, serum cystatin C and HbA1c

Twenty-four-hour urine samples were collected each week after the beginning of HFD treatment. Microalbumin and urinary creatinine levels were measured with Albumin Mouse ELISA Kit (Abcam, Cambridge, MA) and Creatinine Assay Kit (Cayman Chemical, Ann Arbor, MI), according to instructions supplied. Results are expressed as the urine microalbumin to creatinine ratio ($\mu\text{g}/\text{mg}$). The concentration of cystatin C in serum was determined using the mouse DuoSet ELISA kit (R&D Systems) according to the manufacturer's instructions. The percentage of serum HbA1c level was determined by A1CNow[®] (BHR Pharmaceuticals, UK) according to the manufacturer's instructions.

Glucose tolerance test

For glucose tolerance test, after 6 h fasting, blood glucose was measured using a glucometer (Accu-chek; Roche Diagnostic Corporation, Indianapolis, IN) at 0, 15, 30, 60, and 120 min after an intraperitoneal injection of glucose (1 mg/g).

Histological assessment and confocal microscopy

A coronal slice of kidney tissue was fixed in 4% paraformal- dehyde and embedded in paraffin. Tissue was cut at 4 μm and stained with hematoxylin, PAS, and Masson's trichrome. The degree of glomerulosclerosis and interstitial fibrosis were measured using Image J

software (<http://rsb.info.nih.gov/ij/>). The percentage of glomerulosclerosis was calculated by dividing the total area of PAS positive staining in the glomerulus by the total area of the glomerulus. The following antibodies were used: rabbit anti-Tom20 conjugated with Alexa Fluor 647 (Abcam, UK), guinea-pig anti-synaptopodin antibody (Synaptic Systems, GmbH, Goettingen, Germany), followed by goat anti-guinea pig Alexa Fluor 488 (Invitrogen, Mount Waverley, VIC, Australia) and goat anti-Collagen IV (SouthernBiotech, Birmingham, AL) or rabbit anti-fibronectin (Sigma-Aldrich), followed by rabbit-goat Alexa Fluor 488 or goat anti-rabbit Alexa Fluor 488 (Invitrogen). Sections were counterstained with DAPI (4, 6-diamidino-2-phenylindole; Sigma-Aldrich, St Louis, MO) to visualize nuclei. Sections were analyzed with an Olympus Fluoview 1000 confocal microscope (Olympus, Tokyo, Japan), FV10-ASW software (version 1.3c; Olympus), and oil UPLFL × 60 objective (NA 1.25; Olympus). Image J (<http://rsb.info.nih.gov/ij/>) measured the area of staining within the glomerulus tuft. All scoring was performed on blinded slides.

Immunoprecipitation and Western blotting

Kidney tissues, cell culture samples and isolated cells from FACS were sonicated and lysed in 0.4 ml RIPA lysis buffer. The tissue and cell extracts were centrifuged at 3000 rpm at 4°C for 30 minutes to remove cell debris. The protein concentrations were measured by modified Lowry protein assay using BSA as a protein standard (DC protein assay kit, Biorad). Cell lysates (1 mg) were added rabbit anti-Smad4, mouse or rabbit control IgG (Cell Signaling Technology) with gentle rocking overnight at 4°C then immune complex was immunoprecipitated using protein A/G agarose beads (Santa Cruz Biotechnology). In western blotting, proteins were electrophoresed through a 10% SDS-PAGE gel before transferring to a PVDF membrane. After blocking for 30 minutes at 4°C in blocking buffer (5% skim milk powder in PBS with 0.1% Tween 20), the membrane was incubated over night with rabbit anti-synaptopodin, anti-nephrin, anti-PKM2 (Cell Signal Technology), anti-ATPIF1 (Abcam),

MPC-1 (Abcam) or anti-Smad4. The membrane was washed and incubated for 30 minutes at room temperature with a goat anti-rabbit or anti-mouse antibody conjugated with HRP (Cell Signal Technology). After further washing, the membrane was detected with ECL kit (Amersham Pharmacia Biotech, Arlington, IL, USA). α -tubulin and GAPDH were used as internal controls and detected by mouse anti- α -tubulin antibody conjugated with HRP and mouse anti-GAPDH antibody conjugated with HRP.

Isolation of podocytes from mouse kidneys

Kidney tissue from WT or *Smad4*^{-/-} mouse kidneys was digested with collagenase (Sigma). Single-cell suspensions were sequentially labeled with rabbit anti-nephrin (Bioss-USA, Woburn, MA) conjugated with Alexa Fluor 488 fluorophore. Renal nephrin⁺ cells were sorted using BD influx (BD Biosciences) [68]. A total of 8×10^5 to 1.5×10^6 cells/each type were harvested per kidney and analysis with qPCR, western blotting and Seahorse assay.

Lentiviral CRISPR/Cas9 constructs.

For the inducible Smad4 sgRNA constructs, the previously described FgH1tUTG plasmid was modified to contain the Smad4 sgRNA (Smad4 exon4 5' AACAGGTCAGCCGGCCAGTATTC3' and 5' TCCCGAATACTGGCCGGCTGACCT3') cassette, which was inserted into bi-directional BsmB1 sites linked to the GFP fluorescent protein [69]. The constitutive Cas9 expression vectors were derived from the pFUGW, Cas9 protein linked via the T2A peptide to the mCherry fluorescent reporter protein [70].

Smad4 expression retroviral vector constructs

The plasmids encoding Flag-Smad4^{WT}, Flag-Smad4^{L43S} and Flag-Smad4^{R100T} were obtained from the Addgene plasmid repository (Addgene Plasmid #80888, #80889 and

#80891 were gifts from Aristidis Moustakas) [44]. Retroviral vector plasmid encoding Flag-Smad4WT, Flag-Smad4L43S and Flag-Smad4R100T were subcloned into pMSCV-IRES-Puro vector.

Virus Production and Transduction of Podocytes

Viral particles were produced by transient transfection of 293T cells grown in 75cm culture flask with 10 µg of vector DNA along with the packaging constructs pLP1 (5 µg), pLP2 (2.5 µg), and pLP/VSVG (3 µg) (Thermo Fisher) for lentivirus, or Platinum-E packaging cells with 10 µg of vector DNA for retrovirus, using standard calcium phosphate precipitation method. Virus-containing supernatants were collected at 48 hr after transfection and passed through a 0.45-µm filter. Virus were concentrated by precipitation using PEG-6000 [71]. For transduction of podocytes, cells were plated with virus and polybrene (4µg/ml), and incubated overnight at 33°C. Lentivirus-transduced cells were sorted using BD FACSAria™ III by sorting double positive (GFP+/mCherry+) cells. To induce Smad4 sgRNA expression, doxycycline hyclate (Sigma) was dissolved in sterile water at a stock concentration of 10 mg/ml and added to cell culture medium for a final concentration of 1 µg/ml for 24 hours. Retrovirus-transduced cells were selected with 0.6 µg/ml of puromycin in culture media.

Seahorse assay

A Seahorse Bioscience XFe24 Extracellular Flux Analyzer (Seahorse Bioscience, Billerica, MA) was used to measure oxygen consumption rates in real time from podocytes cultured in XFe24 FluxPak Mini cell culture microplates (Seahorse Bioscience) coated with rat tail collagen I (Sigma).

Isolated mouse podocytes were seeded in XF^c24 FluxPak Mini cell culture microplates at a density of 5×10^5 in 300 µl of growth media and differentiated for 7 days. After incubation for a total of 7 days, growth medium was removed and replaced with 500µl of FAO assay

medium prewarmed to 37 °C, supplemented with or without Etomoxir (1µM), cultured at 37°C anaerobic incubator. Measurements of oxygen consumption rates were performed after equilibration in assay medium for 0.5 to 1h. XF Cell Mito Stress Test Kit (Seahorse Bioscience) was used to measure oxygen consumption rates according to the instructions supplied.

Conventional EM sample preparation

Cultured cells were fixed according standard procedures in 2 % glutaraldehyde in sodium cacodylate buffer. Post-fixed with 1% OsO₄, 1.5% K₃Fe(III)(CN)₆. Cells were scraped, pelleted and embedded in 4% ULMP-agarose. Dehydration was done with ethanol and cells were embedded in Epon 812. Ultrathin sections of 70nm were cut on a Leica Ultracut UCT7 and stained with uranyl acetate and lead citrate. EM imaging was done on a Hitachi 7500 TEM.

Measurement of intracellular ROS accumulation

CellROX Deep Red Reagent was from Invitrogen (Carlsbad, CA). Podocytes were treated with normal glucose (1g/L D-glucose) or high glucose (4.5g/L D-glucose) the indicated time intervals, and CellROX Deep Red Reagent was added at a final concentration of 5 µM to the cells and then incubated for 30 min at 37°C. Subsequently, medium was removed, and the cells were washed three times with PBS. The resulting fluorescence was measured using a fluorescence microscope (Axiovert 200M; Zeiss).

SBE4-luciferase reporter assay

One day after SBE4-luciferase plasmid was transfected into *Smad4*^{-/-} podocytes expressing Flag-tagged Smad4 wild type, Smad4 R100T or Smad4 L43S mutant by lipofectamine 2000.

Cells were treated with or without 2ng/ml TGF- β 1 for 8 hours. Then cells were harvested and luciferase assay was performed according to the instruction in luciferase assay kit (Promega).

RNA Extraction and Real-Time RT-qPCR

Total RNA from cultured podocyte samples were isolated and one-step real-time RT-PCR and real-time qPCR performed using SYBR Green PCR Reagents (Sigma), the Thermoscript RT-PCR system (Invitrogen), and the Opticon DNA Engine (MJ Research Inc., South San Francisco, CA), according to manufacturer's instructions. In each reaction, 0.5 μ g of total RNA was reverse transcribed before the following PCR conditions: 94°C for 2 minutes followed by 40 cycles at 94°C for 15 seconds, 58°C for 30 seconds, 72°C for 30 seconds, with final extension at 72°C for 10 minutes. Primers used in this study were: mouse NOX4, fwd 5'- 'cctcctggctgcattagtct-3', rev 5'- ctccgcacaataaaggcaca-3'; collagen IV, fwd 5'- TGACCCTGGTGATGTTCTCA-3', rev 5'-GCCACACCTTGTATGCCTTT; and β -actin, fwd 5'- agacttcgagcaggagatgg -3', rev 5'- caatgcctgggtacatggtg -3'. Amplicon sizes were 225 bp (NOX4) and 266bp (β -actin). The relative amount of mRNA was calculated using the comparative Ct (Δ Ct) method compared with β -actin and expressed as the mean \pm SD.

Cross-linking to determine tetramers, dimers and monomers of PKM2

Isolated cells by FACS or cultured cells were treated with 500- μ M DSS (disuccinimidyl suberate; Thermo Scientific #PI21658), as per the manufacturer's instructions, to cross-link at room temperature [64]. Cell number was counted. Equal numbers of cells were lysed in 4X Bolt LDS Sample Buffer (Invitrogen), boiled for 5 min then western blotting was performed.

Effect of Smad4 deficiency on ATPIF1 mRNA stability

Wild type or Smad4 deficient mouse podocytes were cultured 24 h to normalize PKM2 mRNA expression. Thereafter, 1640 medium was changed and cells were treated with

actinomycin D (5 µg/ml) for 1hr and subsequently incubated with 1640 medium for further 30, 60, 120 and 240 min. Cells were collected and RT-qPCR was performed to quantify ATPIF1 mRNA levels. The following forward (F) and reverse (R) primers were used to amplify mouse ATPIF1 cDNA and β-actin cDNA, respectively. ATPIF1_F: 5'ggttcgggtgtctggggtatg, mouse ATPIF1_R: 5'tcatggtgttcctcagggc, amplicon=193bp; mouse β-actin_F: 5' ccaccatgtaccaggcatt, mouse β-actin_R: 5' actcctgcttgetgatccac, amplicon=177bp.

Quantitative proteomic analysis

The quantitative proteomic analysis was performed according to following procedures. 1. Protein Extraction; 2. Trypsin Digestion; 3. TMT/iTRAQ Labeling; 4. HPLC Fractionation; 5. LC-MS/MS Analysis; 6. Database Search; and 7. Bioinformatics Methods: Gene Ontology (GO) annotation proteome was derived from the UniProt-GOA database (www.ebi.ac.uk/GOA/). Encyclopedia of Genes and Genomes (KEGG) database was used to annotate protein pathway.

Statistical analysis

Data are mean ± SD with statistical analyses performed using Student's t-test, one way or two-way ANOVA from GraphPad Prism 7.0 (GraphPad Software, San Diego, CA) and posthoc Tukey analysis when appropriate. P<0.05 was considered statistically significant.

Author Contributions

Conceived and designed the experiments: JL. Performed the experiments: JL YS WC JF SL XQ SC. Analyzed the data: JL YS WC JF SL XQ QC RC DZ JZ HC SC VO VP PK YR SN

MC HT WC JB DN XY. Contributed reagents/materials/analysis tools: JL. Wrote the paper:
JL YS WC JB DN YX.

Acknowledgments

Supported by the National Health and Medical Research Council of Australia (APP1057581), the National Natural Science Foundation of China (81670667), and Guangdong Medical University of Provincial and Municipal Construction of Colleges and Universities Project (NO. 4SG18001Ga) to J.L; the Major Basic Research Project of Guangdong Province, China (NO. 2017KZDXM041), Guangdong Provincial University Key Platform Featured Innovation Project (Natural Sciences) (NO. 2015KTSCX052), Guangdong Medical University of Provincial and Municipal Construction of Colleges and Universities Project (NO. 4SG18102G and 4SG18056G), and Provincial Preponderant Key Subjects of Public Health and Preventive Medicine Project (NO. 4SG18004G and 4SG17043) to H.T.

Declaration of Interests

The authors have declared that no competing interests exist.

References:

1. National Kidney Foundation, KDOQI Clinical Practice Guideline for Diabetes and CKD: 2012 Update. *Am. J. Kidney Dis.* 60, 850–886 (2012).
2. H. C. Gerstein, et al. Effects of intensive glucose lowering in type 2 diabetes, *N. Engl. J. Med.* 358, 2545–2559 (2008).

3. H.-H. Parving, et al. ALTITUDE Investigators, Cardiorenal end points in a trial of aliskiren for type 2 diabetes, *N. Engl. J. Med.* 367, 2204–2213 (2012).
4. M. Kretzschmar, J. Massagué, SMADs: mediators and regulators of TGF-beta signaling, *Curr. Opin. Genet. Dev.* 8, 103–111 (1998).
5. T. Yamamoto, T. Nakamura, N. A. Noble, E. Ruoslahti, W. A. Border, Expression of transforming growth factor beta is elevated in human and experimental diabetic nephropathy, *Proc. Natl. Acad. Sci. U. S. A.* 90, 1814–1818 (1993).
6. M. M. Shull, et al. Targeted disruption of the mouse transforming growth factor-beta 1 gene results in multifocal inflammatory disease, *Nature* 359, 693–699 (1992).
7. Y. Liu, et al. A critical function for TGF-beta signaling in the development of natural CD4+CD25+Foxp3+ regulatory T cells, *Nat. Immunol.* 9, 632–640 (2008).
8. L. Gorelik, R. A. Flavell, Abrogation of TGFbeta signaling in T cells leads to spontaneous T cell differentiation and autoimmune disease, *Immunity* 12, 171–181 (2000).
9. Zhu Y, Richardson JA, Parada LF, Graff JM (1998), Smad3 mutant mice develop metastatic colorectal cancer. *Cell.* 94(6):703-14.
10. Flanders KC (2004), Smad3 as a mediator of the fibrotic response. *Int J Exp Pathol.* 85(2):47-64.
11. Fujimoto M, Maezawa Y, Yokote K, Joh K, Kobayashi K, Kawamura H, Nishimura M, Roberts AB, Saito Y, Mori S (2003). Mice lacking Smad3 are protected against streptozotocin-induced diabetic glomerulopathy. *Biochem Biophys Res Commun.* 305(4):1002-7.

12. H. Yadav, et al. Protection from obesity and diabetes by blockade of TGF- β /Smad3 signaling, *Cell Metab* 14, 67–79 (2011).
13. C. K. Tan, et al. Smad3 deficiency in mice protects against insulin resistance and obesity induced by a high-fat diet, *Diabetes* 60, 464–476 (2011).
14. Y. B. Y. Sun, et al. Smad3 deficiency protects mice from obesity-induced podocyte injury that precedes insulin resistance, *Kidney Int.* 88, 286–298 (2015).
15. H. Y. Li, et al. Amelioration of high fat diet-induced glucose intolerance by blockade of Smad4 in pancreatic beta-cells, *Exp. Clin. Endocrinol. Diabetes* 123, 221–226 (2015).
16. R. Watts, et al. Increased Smad signaling and reduced MRF expression in skeletal muscle from obese subjects, *Obesity (Silver Spring)* 21, 525–528 (2013). Schiffer. M, et al. Apoptosis in podocytes induced by TGF-beta and Smad7, *J. Clin. Invest.* 108, 807–816 (2001).
17. J. Zhao, S. Miyamoto, Y.-H. You, K. Sharma, AMP-activated protein kinase (AMPK) activation inhibits nuclear translocation of Smad4 in mesangial cells and diabetic kidneys, *AJP: Renal Physiology* 308, F1167–77 (2015).
18. P. Papageorgis, et al. Smad4 inactivation promotes malignancy and drug resistance of colon cancer, *Cancer Res.* 71, 998–1008 (2011).
19. Sauvé M, Hui SK, Dinh DD, Foltz WD, Momen A, Nedospasov SA, Offermanns S, Husain M, Kroetsch JT, Lidington D, Bolz SS. Tumor Necrosis Factor/Sphingosine-1-Phosphate Signaling Augments Resistance Artery Myogenic Tone in Diabetes. *Diabetes.* 2016 Jul;65(7):1916-28.
20. Gu J, Cheng Y, Wu H, Kong L, Wang S, Xu Z, Zhang Z, Tan Y, Keller BB, Zhou H, Wang Y, Xu Z, Cai L. Metallothionein Is Downstream of Nrf2 and Partially Mediates

Sulforaphane Prevention of Diabetic Cardiomyopathy. *Diabetes*. 2017 Feb;66(2):529-542.

doi: 10.2337/db15-1274. Epub 2016 Nov 30

21. Cheng Y, Yu X, Zhang J, Chang Y, Xue M, Li X, Lu Y, Li T, Meng Z, Su L, Sun B, Chen L. Pancreatic kallikrein protects against diabetic retinopathy in KK Cg-Ay/J and high-fat diet/streptozotocin-induced mouse models of type 2 diabetes. *Diabetologia*. 2019 Jun;62(6):1074-1086.

22. Chen X, Han Y, Gao P, Yang M, Xiao L, Xiong X, Zhao H, Tang C, Chen G, Zhu X, Yuan S, Liu F, Dong LQ, Liu F, Kanwar YS, Sun L. Disulfide-bond A oxidoreductase-like protein protects against ectopic fat deposition and lipid-related kidney damage in diabetic nephropathy. *Kidney Int*. 2019 Apr;95(4):880-895.

23. Wu L, Wang K, Wang W, Wen Z, Wang P, Liu L, Wang DW. Glucagon-like peptide-1 ameliorates cardiac lipotoxicity in diabetic cardiomyopathy via the PPAR α pathway. *Aging Cell*. 2018 Aug;17(4):e12763.

24. Spallotta F, Cencioni C, Atlante S, Garella D, Cocco M, Mori M, Mastrocola R, Kuenne C, Guenther S, Nanni S, Azzimato V, et al. Stable Oxidative Cytosine Modifications Accumulate in Cardiac Mesenchymal Cells From Type2 Diabetes Patients: Rescue by α -Ketoglutarate and TET-TDG Functional Reactivation. *Circ Res*. 2018 Jan 5;122(1):31-46.

25. Yu T, Sungelo MJ, Goldberg IJ, Wang H, Eckel RH. Streptozotocin-Treated High Fat Fed Mice: A New Type 2 Diabetes Model Used to Study Canagliflozin-Induced Alterations in Lipids and Lipoproteins. *Horm Metab Res*. 2017 May;49(5):400-406.

26. Lee JY, Jeong EA, Kim KE, Yi CO, Jin Z1, Lee JE, Lee DH, Kim HJ, Kang SS, Cho GJ, Choi WS, Choi SY, Kwon HM, Roh GS. TonEBP/NFAT5 haploinsufficiency attenuates

hippocampal inflammation in high-fat diet/streptozotocin-induced diabetic mice. *Sci Rep.* 2017 Aug 10;7(1):7837.

27. Tatarkiewicz K, Hargrove DM, Jodka CM, Gedulin BR, Smith PA, Hoyt JA, Lwin A, Collins L, Mamedova L, Levy OE, D'Souza L, Janssen S, Srivastava V, Ghosh SS, Parkes DG. A novel long-acting glucose-dependent insulinotropic peptide analogue: enhanced efficacy in normal and diabetic rodents. *Diabetes Obes Metab.* 2014 Jan;16(1):75-85.

28. Neumann UH, Ho JSS, Chen S, Tam YYC, Cullis PR, Kieffer TJ. Lipid nanoparticle delivery of glucagon receptor siRNA improves glucose homeostasis in mouse models of diabetes. *Mol Metab.* 2017 Oct;6(10):1161-1172.

29. H. J. Zhao, et al. Endothelial nitric oxide synthase deficiency produces accelerated nephropathy in diabetic mice, *J. Am. Soc. Nephrol.* 17, 2664–2669 (2006).

30. D. A. Yuen, et al. eNOS deficiency predisposes podocytes to injury in diabetes, *J. Am. Soc. Nephrol.* 23, 1810–1823 (2012).

31. Kanetsuna Y, Takahashi K, Nagata M, Gannon MA, Breyer MD, Harris RC, Takahashi T (2007). Deficiency of endothelial nitric-oxide synthase confers susceptibility to diabetic nephropathy in nephropathy-resistant inbred mice. *Am J Pathol.* 2007,170(5):1473-84

32. Braasch D. A, Corey D. R., Locked nucleic acid (LNA): fine-tuning the recognition of DNA and RNA, *Chem. Biol.* 8, 1–7 (2001).

33. M. Petersen, J. Wengel, LNA: a versatile tool for therapeutics and genomics, *Trends Biotechnol.* 21, 74–81 (2003).

34. A. Grünweller, R. K. Hartmann, Locked nucleic acid oligonucleotides: the next generation of antisense agents? *BioDrugs* 21, 235–243 (2007).

35. O. R. Mook, F. Baas, M. B. de Wissel, K. Fluiter, Evaluation of locked nucleic acid-modified small interfering RNA in vitro and in vivo, *Mol Cancer Ther* 6, 833–843 (2007).
36. K. S. Schmidt, et al. Application of locked nucleic acids to improve aptamer in vivo stability and targeting function, *Nucleic Acids Res* 32, 5757–5765 (2004).
37. M. E. Gallo Cantafio, et al. Pharmacokinetics and Pharmacodynamics of a 13-mer LNA-inhibitor-miR-221 in Mice and Non-human Primates, *Mol Ther Nucleic Acids* 5, e326 (2016).
38. S. A. Moschos, et al. Uptake, efficacy, and systemic distribution of naked, inhaled short interfering RNA (siRNA) and locked nucleic acid (LNA) antisense, *Mol Ther* 19, 2163–2168 (2011).
39. Ryan D, Sutherland MR, Flores TJ, Kent AL, Dahlstrom JE, Puelles VG, Bertram JF, McMahon AP, Little MH, Moore L, Black MJ. Development of the Human Fetal Kidney from Mid to Late Gestation in Male and Female Infants. *EBioMedicine*. 2018 , 27:275-283.
40. Puelles VG, Cullen-McEwen LA, Taylor GE2, Li J, Hughson MD, Kerr PG, Hoy WE, Bertram JF. Human podocyte depletion in association with older age and hypertension. *Am J Physiol Renal Physiol*. 2016, 310(7):F656-F668.
41. S. Ozawa, et al. Glycolysis, but not Mitochondria, responsible for intracellular ATP distribution in cortical area of podocytes, *Sci Rep* 5, 18575 (2015).
42. K Khazim, et al. The antioxidant silybin prevents high glucose-induced oxidative stress and podocyte injury in vitro and in vivo. *Am J Physiol Renal Physiol*. 305(5):F691-700 (2013)

43. Y Gorin, et al. Targeting NADPH oxidase with a novel dual Nox1/Nox4 inhibitor attenuates renal pathology in type 1 diabetes. *Am J Physiol Renal Physiol.* 308(11):F1276-87 (2015)
44. Jha JC, Thallas-Bonke V, Banal C, Gray SP, Chow BS, Ramm G, Quaggin SE, Cooper ME, Schmidt HH, Jandeleit-Dahm KA. Podocyte-specific Nox4 deletion affords renoprotection in a mouse model of diabetic nephropathy. *Diabetologia.*59(2):379-89 (2016).
45. Dombrauckas JD, Santarsiero BD, Mesecar AD. Structural basis for tumor pyruvate kinase M2 allosteric regulation and catalysis. *Biochemistry.* 2005 Jul 12;44(27):9417-29.
46. Morén A, Itoh S, Moustakas A, Dijke P, Heldin CH. Functional consequences of tumorigenic missense mutations in the amino-terminal domain of Smad4. *Oncogene.* 2000 Sep 7;19(38):4396-404.
47. Bindea G, et al. a Cytoscape plug-in to decipher functionally grouped gene ontology and pathway annotation networks. *Bioinformatics* 25,1091–1093 (2009).
48. García-Aguilar A, Cuezva JM. A Review of the Inhibition of the Mitochondrial ATP Synthase by IF1 in vivo: Reprogramming Energy Metabolism and Inducing Mitohormesis. *Front Physiol.* 2018 Sep 19;9:1322.
49. Shen L, Zhi L, Hu W, Wu MX. IEX-1 targets mitochondrial F1Fo-ATPase inhibitor for degradation. *Cell Death Differ.* 2009 Apr;16(4):603-12.
50. Y. Abe, Tet al. Bioenergetic characterization of mouse podocytes, *Am. J. Physiol., Cell Physiol.* 299, C464–76 (2010).
51. P. Bhargava, R. G. Schnellmann, Mitochondrial energetics in the kidney, *Nature reviews. Nephrology* 13, 629–646 (2017).

52. D. L. Galvan, N. H. Green, F. R. Danesh, The hallmarks of mitochondrial dysfunction in chronic kidney disease, *Kidney Int.* 92, 1051–1057 (2017).
53. X. X. Wang, et al. G Protein-Coupled Bile Acid Receptor TGR5 Activation Inhibits Kidney Disease in Obesity and Diabetes, *J. Am. Soc. Nephrol.* 27, 1362–1378 (2016).
54. N. Shirata, et al. Glomerulosclerosis Induced by Deficiency of Membrane-Associated Guanylate Kinase Inverted 2 in Kidney Podocytes, *J. Am. Soc. Nephrol.* 28, 2654–2669 (2017).
55. Williamson JR, Steinman R, Coll K, Rich TL (1981) Energetics of citrulline synthesis by rat liver mitochondria. *J Biol Chem.* 256(14):7287-97.
56. Pullman, M. E., and Monroy, G. C. (1963). A Naturally occurring inhibitor of mitochondrial Adenosine Triphosphatase. *J. Biol. Chem.* 238, 3762–3769.
57. García-Bermúdez J, et al. PKA Phosphorylates the ATPase Inhibitory Factor 1 and Inactivates Its Capacity to Bind and Inhibit the Mitochondrial H(+)-ATP Synthase. *Cell Rep.* 2015 Sep 29;12(12):2143-55.
58. Sánchez-Cenizo L, et al. Up-regulation of the ATPase inhibitory factor 1 (IF1) of the mitochondrial H⁺-ATP synthase in human tumors mediates the metabolic shift of cancer cells to a Warburg phenotype. *J Biol Chem.* 2010 Aug 13;285(33):25308-13.
59. Chen WW, et al. Inhibition of ATP1F1 ameliorates severe mitochondrial respiratory chain dysfunction in mammalian cells. *Cell Rep.* 2014 Apr 10;7(1):27-34.
60. Dunlop M, Aldose reductase and the role of the polyol pathway in diabetic nephropathy, *Kidney Int. Suppl.* 77, S3–12 (2000).

61. Giacco F, et al. Knockdown of glyoxalase 1 mimics diabetic nephropathy in nondiabetic mice, *Diabetes* 63, 291–299 (2014).
62. Fogo A.B, The targeted podocyte, *J. Clin. Invest.* 121, 2142–2145 (2011).
63. Reidy K, Kang H.M, Hostetter T, Susztak K, Molecular mechanisms of diabetic kidney disease, *J. Clin. Invest.* 124, 2333–2340 (2014).
64. Qi W., et al. Pyruvate kinase M2 activation may protect against the progression of diabetic glomerular pathology and mitochondrial dysfunction, *Nat. Med.* 54, 2188 (2017).
65. L. Pang, T. Qiu, X. Cao, M. Wan, Apoptotic role of TGF- β mediated by Smad4 mitochondria translocation and cytochrome c oxidase subunit II interaction, *Exp. Cell Res.* 317, 1608–1620 (2011).
66. L. Zhu, et al. The mitochondrial protein CHCHD2 primes the differentiation potential of human induced pluripotent stem cells to neuroectodermal lineages, *J. Cell Biol.* 215, 187–202 (2016).
67. Janssen HL, Reesink HW, Lawitz EJ, Zeuzem S, Rodriguez-Torres M, Patel K, van der Meer AJ, Patick AK, Chen A, Zhou Y, Persson R, King BD, Kauppinen S, Levin AA, Hodges MR. Treatment of HCV infection by targeting microRNA. *N Engl J Med.* 2013 May 2;368(18):1685-94.
68. Sun YB, Qu X, Howard V, Dai L, Jiang X, Ren Y, Fu P, Puelles VG, Nikolic-Paterson DJ, Caruana G, Bertram JF, Sleeman MW, Li J. Smad3 deficiency protects mice from obesity-induced podocyte injury that precedes insulin resistance. *Kidney Int.* 2015 Aug;88(2):286-98.

69. Aubrey BJ, Kelly GL, Kueh AJ, Brennan MS, O'Connor L, Milla L, Wilcox S, Tai L, Strasser A, Herold MJ. An inducible lentiviral guide RNA platform enables the identification of tumor-essential genes and tumor-promoting mutations in vivo. *Cell Rep.* 2015 Mar 3;10(8):1422-32.
70. Lois C, Hong EJ, Pease S, Brown EJ, Baltimore D. Germline transmission and tissue-specific expression of transgenes delivered by lentiviral vectors. *Science.* 2002 Feb 1;295(5556):868-72.
71. Kutner RH, Zhang XZ, Reiser J, Production, concentration and titration of pseudotyped HIV-1-based lentiviral vectors, *Nat Protoc* 4, 495–505 (2009).

Figure legends

Figure 1. *Smad4* LNA decreases *Smad4* expression and halts the progression of type 2 diabetic nephropathy. (A) Western blotting demonstrated *Smad4* expression levels in mouse podocytes 4 days after *Smad4* LNA or CTL LNA treatment. (B) Schema illustrating administration of *Smad4* LNA or CTL LNA in model of type II diabetic nephropathy in eNOS deficient mice. (C) Western blotting demonstrated expression levels of *Smad4*, *Smad3*, PKM2 and α -Tubulin after 6-week *Smad4* LNA or CTL LNA treatment in age-matched kidney or type 2 diabetic nephropathy. (D) Western blotting demonstrated expression levels of *Smad4* in WT, *Smad4* KO (KO), control LNA-treated WT and *Smad4* LNA-treated WT podocytes. (E) Quantification of expression levels of *Smad4*, *Smad3*, PKM2 and α -Tubulin after 6-week *Smad4* LNA or CTL LNA treatment in age-matched kidney or type 2 diabetic nephropathy. Western blotting demonstrated expression levels of *Smad4* and GAPDH in lung (F), spleen (G) and liver (H) in age-matched mice, 6-week *Smad4* LNA-treated or CTL LNA-treated mice. (I) HbA1C after *Smad4* LNA or CTL LNA treatment. (J) Quantification of p57⁺ cells per Glomerular Cross Section (GCS) in age-matched, 6-week *Smad4* LNA-treated or CTL LNA-treated mouse kidneys. (K) Quantification of staining area of synaptopodin in glomeruli in age-matched, 6-week *Smad4* LNA-treated or CTL LNA-treated mouse kidneys. (L-N) PAS staining demonstrating age-matched kidney, CTL LNA treated diabetic nephropathy and *Smad4* LNA-treated diabetic nephropathy. Quantification of collagen IV staining (O), urinary albumin/creatinine ratio (P) and; serum Cystatin C levels (Q) in age-matched mice, CTL LNA treated or *Smad4* LNA-treated mice with type 2 diabetic nephropathy. Two-way ANOVA, data are mean \pm s.d. from groups of eight mice. * $P < 0.05$; *** $P < 0.01$; **** $P < 0.001$; N.S, not significant, $P > 0.05$.

Figure 2. *Smad4* expression is increased in human and mouse diabetic nephropathy. (A&B) Confocal microscopy demonstrated WT1 (green), *Smad4* (red), Tom20 (green), DAPI (blue) and merged images in normal human kidney (A), renal biopsy with diabetic nephropathy (B). Digital enlargement of normal human kidney (C, E) and diabetic nephropathy (D, F). Of note, localization of WT1 and *Smad4*, and *Smad4* and Tom20. Confocal microscopy demonstrated synaptopodin (green), *Smad4* (red), Tom20 (green), DAPI (blue) and merged images in normal mouse kidney (G) or diabetic nephropathy (H). Digital enlargement of age-matched mouse kidney (I, K) and diabetic nephropathy (J, L). Of note, localization of synaptopodin and *Smad4*, and *Smad4* and Tom20. (M) Nephrin (+) cells were isolated by FACS from mouse kidneys. Western blotting demonstrated *Smad4* expression in isolated nephrin (+) cells (N, O).

Figure 3. *Smad4* deficiency in podocytes reduces kidney injury in type 2 diabetic nephropathy. (A) Western blotting demonstrating expression levels of *Smad4*, synaptopodin and GAPDH in nephrin (+) cells isolated from $eNOS^{-/-}$ PodCre ND, $eNOS^{-/-}$ PodCre HFD+STZ, $eNOS^{-/-}$ PodCre-*Smad4*^{-/-} ND and $eNOS^{-/-}$ PodCre-*Smad4*^{-/-} HFD+STZ treated mouse kidneys. (B) Quantification of p57⁺ cells per Glomerular Cross Section (GCS) in $eNOS^{-/-}$ PodCre ND, $eNOS^{-/-}$ PodCre HFD+STZ, $eNOS^{-/-}$ PodCre-*Smad4*^{-/-} ND and $eNOS^{-/-}$ PodCre-*Smad4*^{-/-} HFD+STZ treated mouse kidneys. (C) Western blotting demonstrating expression levels of nephrin and α -Tubulin in $eNOS^{-/-}$ PodCre ND, $eNOS^{-/-}$ PodCre HFD+STZ, $eNOS^{-/-}$ PodCre-*Smad4*^{-/-} ND and $eNOS^{-/-}$ PodCre-*Smad4*^{-/-} HFD+STZ treated mouse kidneys. (D) Quantification of ratios of nephrin/ α -Tubulin in western blotting. (E) Periodic acid–Schiff (PAS) staining of sections from ND-treated or HFD+STZ-treated $eNOS^{-/-}$ PodCre or $eNOS^{-/-}$ PodCre-*Smad4*^{-/-} mouse kidneys. (F) Confocal microscopy demonstrated collagen IV

expression in ND-treated or HFD+STZ-treated *eNOS*^{-/-}PodCre or *eNOS*^{-/-}PodCre-Smad4^{-/-} mouse kidneys. Quantitation of collagen IV staining area/glomerular cross-section (G), serum Cystatin C levels (H) and urinary albumin/creatinine ratio (I) in ND-treated or HFD+STZ-treated *eNOS*^{-/-}PodCre mouse or *eNOS*^{-/-}PodCre-Smad4^{-/-} mouse kidneys. Data are mean \pm s.d. from groups of eight mice. **P*<0.05, ***P*<0.01, ****P*<0.001.

Figure 4. *Smad4* deficiency increases glycolysis and lactate production, decreases reactive oxygen species and protects podocytes from high glucose-induced injury. Wild type (WT) and *Smad4* KO mouse podocytes were treated with normal glucose (NG, 1g/L D-glucose) or high glucose (HG, 4.5g/L D-glucose) for 24 hrs then Seahorse was performed. Seahorse demonstrated real-time changes of ECAR in WT and *Smad4* KO podocytes after treatment with glucose, oligomycin and 2-Deoxy-D-glucose (2-DG) (A). Quantification of non-glycolytic acidification, glycolysis, glycolytic capacity and glycolytic reserve (B). Seahorse demonstrated real-time changes of oxygen consumption rate (OCR) after treatment with oligomycin, FCCP and rotenone in WT and *Smad4* KO podocytes (C). Quantification of basal, maximal, ATP-linked respiration and reserve capacity (D). All values are means \pm SD of at least three independent experiments. N.S, Not Significant, *P*>0.05; **P*< 0.05; ***P*< 0.01; ****P*< 0.001; *****P*< 0.0001. Electron Microscopy demonstrated mitochondria morphology in WT (E) and *Smad4* KO (F) podocytes. (G) PCR demonstrated relative mitochondrial copy number in WT and *Smad4* KO podocytes. (H) Western blotting demonstrated expression of *Smad4*, HK1, PKM2, FPKL, PGC-1 α and α -tubulin in WT and *Smad4* KO podocytes. Lactate production in WT or *Smad4* KO podocytes under high glucose (HG) and normal glucose (NG) conditions (I, J). Relative fluorescence intensities of reactive oxygen species (ROS) under normal glucose (NG) or high glucose (HG) condition in podocytes (K). Relative fluorescence intensities of ROS after 24-hour NG, HG or NG+ D-

mannitol treatment in podocytes (L). Relative fluorescence intensities of ROS after 24-hour NG or HG treatment in WT or Smad4 KO podocytes (M). Western blotting demonstrated NOX4 and synaptopodin expression after 24-hour NG or HG treatment in WT or Smad4 KO podocytes (N). All values are means \pm SD of at least three independent experiments. * $P < 0.05$, ** $P < 0.01$, *** $P < 0.001$, **** $P < 0.0001$.

Figure 5. Smad4 interacts with rate-limiting glycolytic enzyme PKM2 to modulate PKM2 tetramer formation and regulate lactate production in podocytes. WB demonstrated expression levels of ATPIF1 and PKM2 in age-matched kidneys and 16-week type 2 diabetic nephropathy (A). Quantitation of arbitrary ratios of ATPIF1 and PKM2 to α -Tubulin (B). Immunoprecipitation (IP)/WB demonstrated the interactions between Smad4 and ATPIF1 and PKM2 in nephrin⁺ podocytes isolated from age-matched kidneys and 16-week type 2 diabetic nephropathy (C). Quantitation of arbitrary ratios of ATPIF1 and PKM2 to Smad4 (D). Lactate production in different periods of under high glucose treatment in podocytes (upper panel), IP/WB demonstrated interaction between Smad4 and PKM2 after 4-, 12- and 24-hour HG treatment in podocytes (lower panel) (E). PKM2 activities in wild type (WT), Smad4 KO (KO) mouse podocytes under normal glucose (NG), high glucose (HG) or D-mannitol (D-M) treatment for 24 hours (F). Western blotting demonstrated PKM2 tetramer, dimer and monomer after normal glucose (NG), high glucose (HG) or D-mannitol (D-M) treatment for 24 hours in wild type (WT) or Smad4 KO (KO) mouse podocytes after cross-linking treatment (G). Quantification of ratios of Tetramer/Dimer+Monomer. * $P < 0.05$; ** $P < 0.01$ (H). 293T cells were transduced with FlagPKM2, HASmad4 and empty vector with various dosages. After 48 hours, cells were collected for Western blotting (upper panel), Immunoprecipitation/Western blotting (middle panel) and cross-linking/Western blotting (lower panel). Western blotting demonstrated expression levels of HA-Smad4 (upper panel),

interactions of FlagPKM2 with HASmad4 (middle panel) and FlagPKM2 tetramer, dimer and monomer (lower panel) (I). Smad4 KO podocytes were transduced with an empty retroviral vector, or retroviral vectors over-expressing Smad4 WT, Smad4 R100T, or Smad4 L43S. SBE4-Luciferase assay demonstrated transcription activities in Smad4 KO, Smad4 WT, Smad4 R100T and Smad4 L43S podocytes with or without TGF- β 1 treatment (J). IP/WB demonstrated interaction between Smad4 and PKM2 after 24-hour NG or HG treatment in WT, R100T and L43S podocytes (K). Cross-linking/Western blotting demonstrated PKM2 tetramer, dimer and monomer after 24-hour NG or HG treatment in WT, R100T and L43S podocytes (L). Lactate production in WT, R100T, L43S and Smad4 KO podocytes after 24-hour NG or HG treatment (M). CellRox Deep Red test demonstrated relative fluorescence intensity in WT, R100T, L43S and Smad4 KO podocytes treated with NG or HG for 24 hrs (N). WB demonstrated expression levels of Synaptopodin, Smad4 and GAPDH in WT, R100T, L43S and Smad4 KO podocytes treated with NG or HG for 24 hrs (O). RT-qPCR demonstrated ratios of Nox4/ β -actin in WT, R100T, L43S and Smad4 KO podocytes treated with NG or HG for 24 hrs (P). One-way ANOVA, all values are means \pm SD of at least three independent experiments. ** $P < 0.01$; **** $P < 0.0001$; * $P < 0.05$ vs WT or vs R100T or L43S under HG condition; *** $P < 0.0001$ vs WT or vs R100T or L43S under NG or HG condition. N.S, not significant, $P > 0.05$.

Fig 6. Quantitative proteomic profiling for wild type (WT) and Smad4 knockout (KO) mouse podocytes under normal glucose (NG) or high glucose (HG) treatment. (A) Volcano plot of the protein abundance changes in response to NG or HG in WT or Smad4 KO podocytes. Average protein expression ratio of 3 replicates (log 2 transformed) between KO+NG vs WT+NG and KO+HG vs WT+HG. Different treatment groups were plotted against p-value by t-test ($-\log_{10}$ transformed). Cutoff of $p = 0.05$ and 1.3-fold change were marked by blue

and red dots, respectively. (B) Functional annotation of altered proteome in four experimental groups. A GO analysis of the significantly changed proteins identified in proteomic analysis for biological process, molecular function, and KEGG pathway. (C) The figure shows protein access number, gene name, ratio and p value in four experiment groups in quantitative Mass Spectrometry.

Figure 7. *Smad4* interacts with *ATPIF1* to regulate the activity of mitochondrial oxidative phosphorylation in mouse podocytes. (A) Western blotting (WB) demonstrated the expression levels of *Smad4*, *Synaptopodin*, *ATPIF1*, *MPC1* and α -Tubulin in *Smad4* deficient and wild type mouse podocytes under normal glucose (1g/L D-glucose, NG) or high glucose (4.5g/L D-glucose HG) condition. (B) Relative ATP levels in *Smad4* WT, *Smad4* R100T, *Smad4* L43S or *Smad4* KO podocytes treated with NG or HG for 24 hours. All values are means \pm SD of at least three independent experiments. * $P < 0.05$, ** $P < 0.01$, *** $P < 0.001$. N.S, $P > 0.05$. (C) RT-qPCR demonstrated relative mRNA levels of *ATPIF1* in WT or *Smad4* KO mouse podocytes treated with NG or HG for 24hrs. (D) Decay curves demonstrated *ATPIF1* mRNA half-life 30, 60, 120 and 140 mins after wild type (WT) or *Smad4* knockout (KO) mouse podocyte were treated with 5 μ g/ml actinomycin D. (E) Western blotting demonstrated *ATPIF1* expression levels in wild type or *Smad4* KO mouse podocytes after treatment with 0.5 mM o-phe for 1hr, or treatment with o-phe then removal of o-phe and treatment with 20 μ g/ml cycloheximide for different periods of time as indicated. (F) Decay curves demonstrated *ATPIF1* protein half-life after wild type (WT) or *Smad4* knockout (KO) mouse podocyte were treated with 0.5 mM o-phenanthroline (o-phe) for 1 hr then o-phe was replaced with 20 μ g/ml cycloheximide for different periods of time. (G) Doxycycline (Dox) inducible sgRNA cassette/cas9 system to delete *Smad4* gene was employed in mouse podocytes. WB and IP/WB demonstrated that expression of *Smad4* and *ATPIF1* and the interaction between *Smad4* and

ATPIF1 decrease following Dox treatment. Seahorse demonstrated oxygen consumption rate (OCR) in Basal (H), Maximal (I) and ATP-linked Respiration (J) in WT or Dox-inducible sgRNA cassette/cas9 system in podocytes treated with different dosages of Dox. (K-N) *Smad4* KO podocytes were transduced with an empty retroviral vector; or retroviral vectors over-expressing *Smad4* WT, *Smad4* R100T, or *Smad4* L43S. Western blotting demonstrated expression levels of *Smad4*, *ATPIF1* and β -actin (K). IP/WB demonstrated interaction between *Smad4* and *ATPIF1* in *Smad4* WT, *Smad4* R100T, and *Smad4* L43S podocytes (K). Seahorse demonstrated OCR in Basal (L), Maximal (M) and ATP-linked Respiration (N) in *Smad4* WT, *Smad4* R100T, *Smad4* L43S or *Smad4* KO podocytes. All values are means \pm SD of at least three independent experiments. * $P < 0.05$, ** $P < 0.01$, *** $P < 0.001$. N.S, $P > 0.05$.

Suppl. Fig 1. (A) Schema illustrating mouse model of type II diabetic nephropathy using high fat diet (HFD) and a single dose streptozotocin (50mg/Kg) intraperitoneal injection. (B) Increment change of body weight in *eNOS*^{+/+} ND, *eNOS*^{+/+} HFD+STZ, *eNOS*^{-/-} ND and *eNOS*^{-/-} HFD+STZ. (C, D) HbA1c% (C) and plasma insulin level (D) change in *eNOS*^{+/+} ND, *eNOS*^{+/+} HFD+STZ, *eNOS*^{-/-} ND and *eNOS*^{-/-} HFD+STZ after 24 weeks of treatment. (E) Periodic acid–Schiff (PAS) staining of sections from *eNOS*^{+/+} ND, *eNOS*^{+/+} HFD+STZ, *eNOS*^{-/-} ND and *eNOS*^{-/-} HFD+STZ mouse kidneys. (F) Urinary albumin/creatinine ratio changes from *eNOS*^{+/+} ND, *eNOS*^{+/+} HFD+STZ, *eNOS*^{-/-} ND and *eNOS*^{-/-} HFD+STZ mouse. (H) Serum cystatin C changes from *eNOS*^{+/+} ND, *eNOS*^{+/+} HFD+STZ, *eNOS*^{-/-} ND and *eNOS*^{-/-} HFD+STZ mouse. Data are mean \pm s.d. from groups of eight mice. * $P < 0.05$, ** $P < 0.01$, *** $P < 0.001$.

Suppl. Fig 2. *Smad4* LNA administration retards the progression of mouse type 2 diabetic nephropathy. (A-C) changes in body weight, fasting blood glucose levels, and plasma insulin in age-matched, control-LNA (CTL-LNA)-treated or *Smad4* LNA-treated in type 2 diabetic *eNOS*^{-/-} mice. Glucose tolerance test (E) and quantification of Glucose tolerance test (D) in age-matched, control-LNA (CTL-LNA)-treated or *Smad4* LNA-treated in type 2 diabetic *eNOS*^{-/-} mice. Data are mean ± s.d. from groups of 6 mice. One way ANOVA.

Suppl. Fig 3. *Smad4* LNA treatment decreases podocyte injury and glomerulosclerosis in type 2 diabetic nephropathy. Confocal microscopy demonstrated synaptopodin (red, A-C) collagen IV expression (green, D-F) in age-matched kidney, CTL LNA treated diabetic nephropathy and *Smad4* LNA-treated diabetic nephropathy.

Suppl. Fig 4. *Smad4* deficiency in podocytes protects mice from type 2 diabetic nephropathy. (A-D) changes in body weight, fasting blood glucose levels, HbA1c and plasma insulin in ND-treated or HFD+STZ-treated *eNOS*^{-/-} PodCre mice or *eNOS*^{-/-} PodCre-*Smad4*^{-/-} mice. Glucose tolerance test (E) and quantification of Glucose tolerance test (F) in ND-treated or HFD+STZ-treated *eNOS*^{-/-} PodCre mice or *eNOS*^{-/-} PodCre-*Smad4*^{-/-} mice. Data are mean ± s.d. from groups of eight mice. N.S, $P > 0.05$; * $P < 0.05$; ** $P < 0.01$; *** $P < 0.001$.

Suppl. Fig 5. Encyclopedia of Genes and Genomes (KEGG) database annotates protein pathways in wild type or *Smad4* deficient podocytes treated with normal glucose or high glucose.

Fig. 1

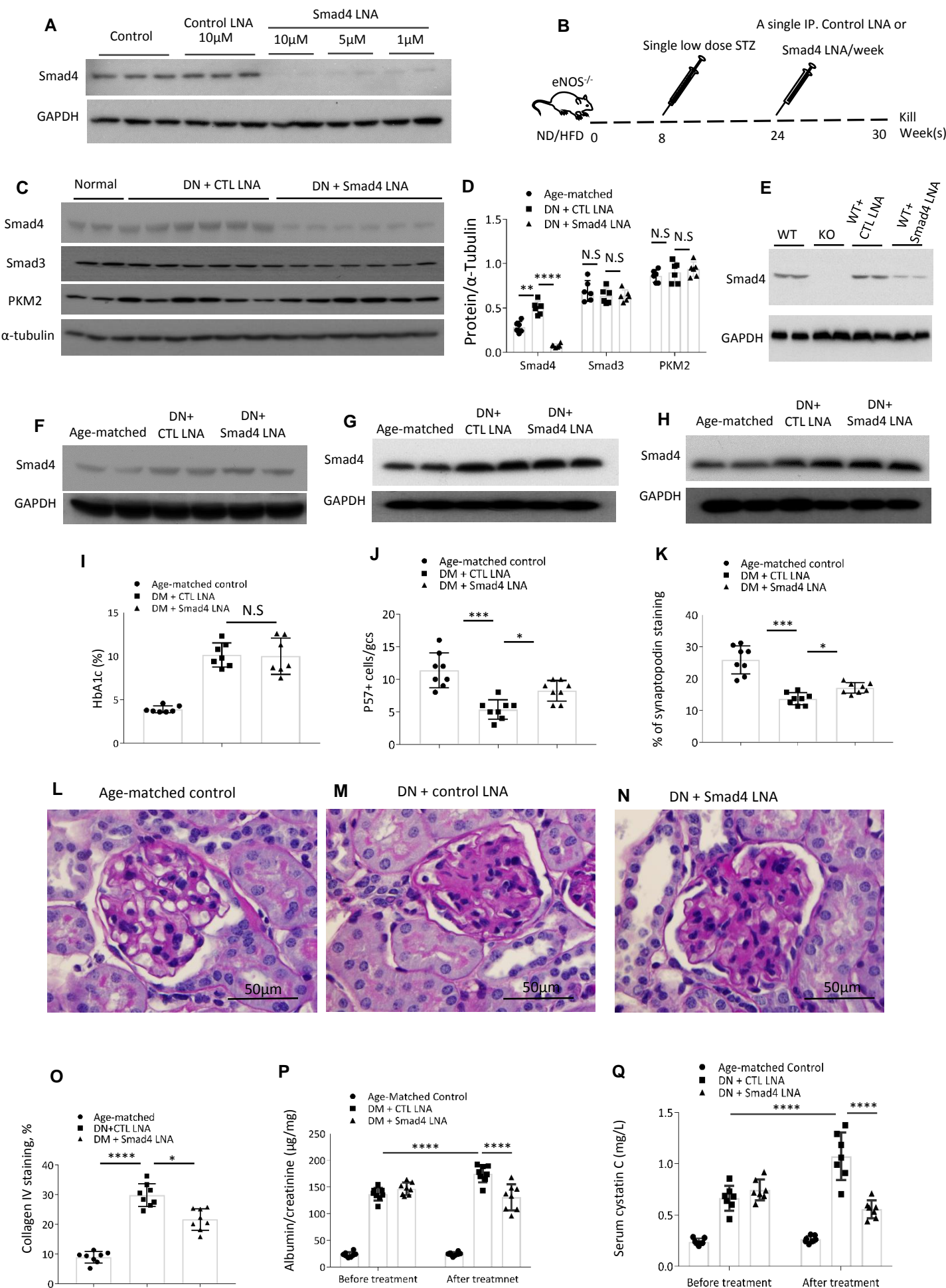


Figure 1. *Smad4* LNA decreases *Smad4* expression and halts the progression of type 2 diabetic nephropathy. (A) Western blotting demonstrated *Smad4* expression levels in mouse podocytes 4 days after *Smad4* LNA or CTL LNA treatment. (B) Schema illustrating administration of *Smad4* LNA or CTL LNA in model of type II diabetic nephropathy in *eNOS* deficient mice. (C) Western blotting demonstrated expression levels of *Smad4*, *Smad3*, *PKM2* and α -Tubulin after 6-week *Smad4* LNA or CTL LNA treatment in age-matched kidney or type 2 diabetic nephropathy. (D) Western blotting demonstrated expression levels of *Smad4* in WT, *Smad4* KO (KO), control LNA-treated WT and *Smad4* LNA-treated WT podocytes. (E) Quantification of expression levels of *Smad4*, *Smad3*, *PKM2* and α -Tubulin after 6-week *Smad4* LNA or CTL LNA treatment in age-matched kidney or type 2 diabetic nephropathy. Western blotting demonstrated expression levels of *Smad4* and *GAPDH* in lung (F), spleen (G) and liver (H) in age-matched mice, 6-week *Smad4* LNA-treated or CTL LNA-treated mice. (I) HbA1C after *Smad4* LNA or CTL LNA treatment. (J) Quantification of p57⁺ cells per Glomerular Cross Section (GCS) in age-matched, 6-week *Smad4* LNA-treated or CTL LNA-treated mouse kidneys. (K) Quantification of staining area of synaptopodin in glomeruli in age-matched, 6-week *Smad4* LNA-treated or CTL LNA-treated mouse kidneys. (L-N) PAS staining demonstrating age-matched kidney, CTL LNA treated diabetic nephropathy and *Smad4* LNA-treated diabetic nephropathy. Quantification of collagen IV staining (O), urinary albumin/creatinine ratio (P) and; serum Cystatin C levels (Q) in age-matched mice, CTL LNA treated or *Smad4* LNA-treated mice with type 2 diabetic nephropathy. Two-way ANOVA, data are mean \pm s.d. from groups of eight mice. * $P < 0.05$; *** $P < 0.01$; **** $P < 0.001$; N.S, not significant, $P > 0.05$.

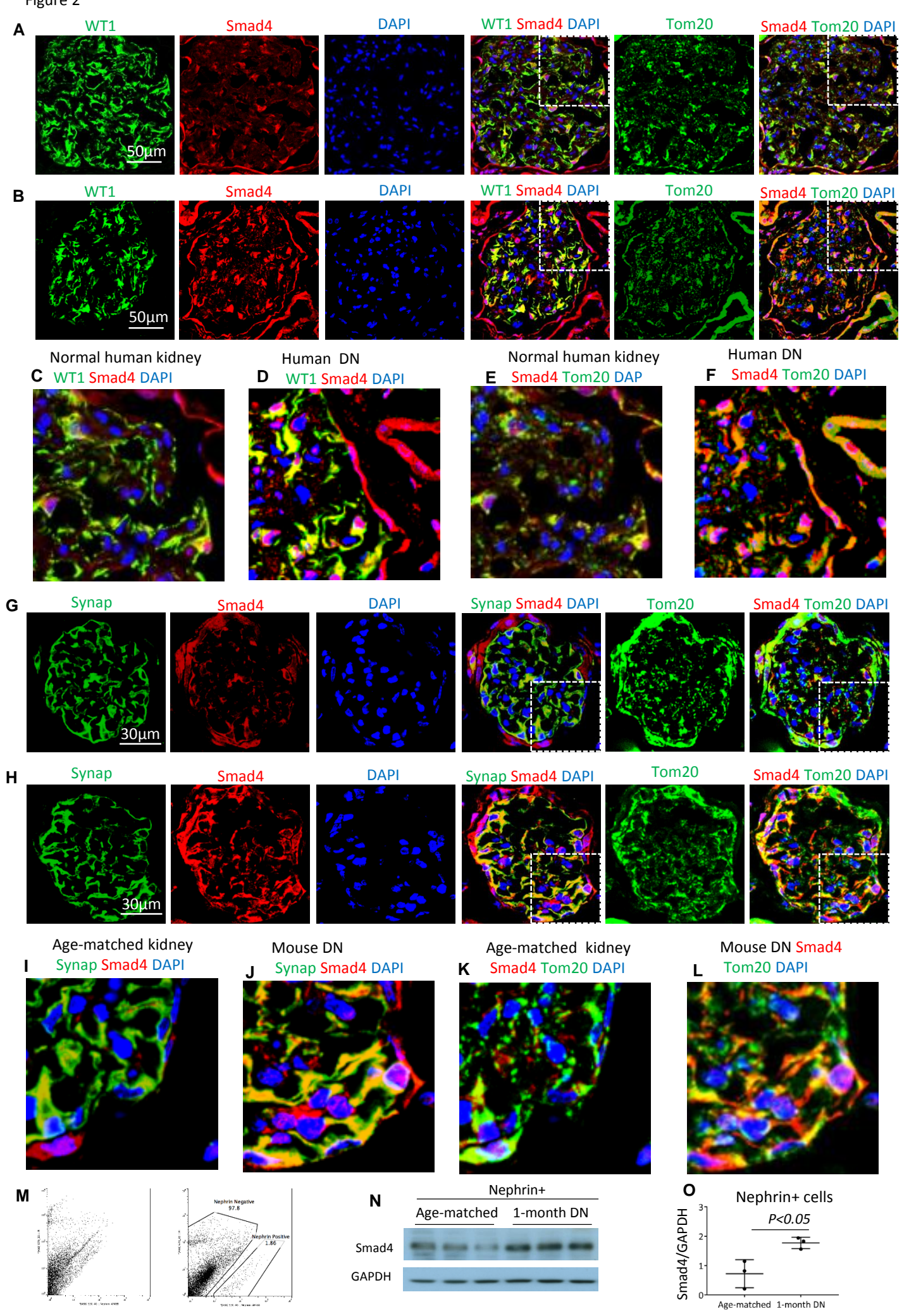


Figure 2. *Smad4* expression is increased in human and mouse diabetic nephropathy. (A&B) Confocal microscopy demonstrated WT1 (green), *Smad4* (red), Tom20 (green), DAPI (blue) and merged images in normal human kidney (A), renal biopsy with diabetic nephropathy (B). Digital enlargement of normal human kidney (C, E) and diabetic nephropathy (D, F). Of note, localization of WT1 and *Smad4*, and *Smad4* and Tom20. Confocal microscopy demonstrated synaptopodin (green), *Smad4* (red), Tom20 (green), DAPI (blue) and merged images in normal mouse kidney (G) or diabetic nephropathy (H). Digital enlargement of age-matched mouse kidney (I, K) and diabetic nephropathy (J, L). Of note, localization of synaptopodin and *Smad4*, and *Smad4* and Tom20. (M) Nephrin (+) cells were isolated by FACS from mouse kidneys. Western blotting demonstrated *Smad4* expression in isolated nephrin (+) cells (N, O).

Figure 3

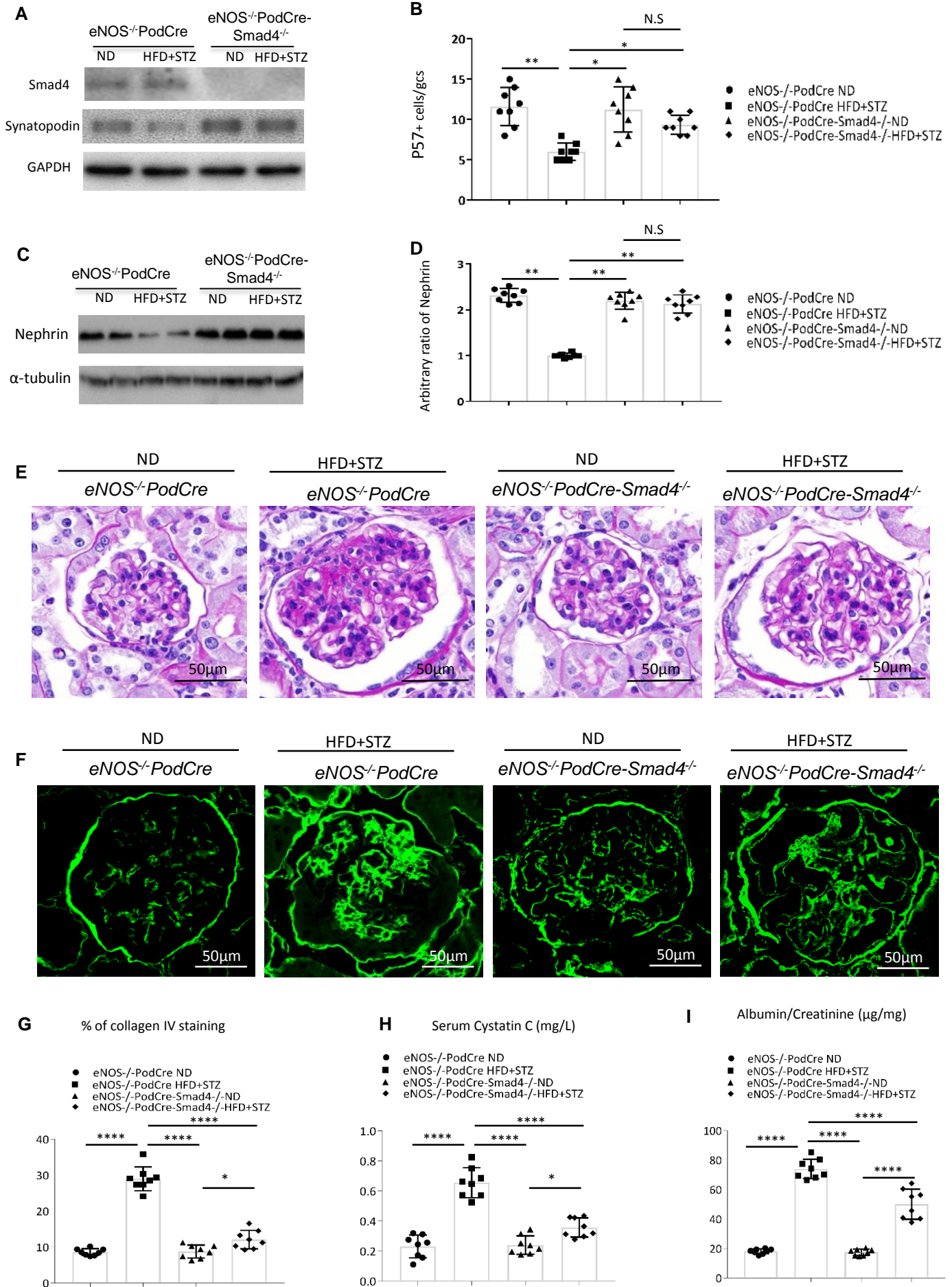


Figure 3. *Smad4* deficiency in podocytes reduces kidney injury in type 2 diabetic nephropathy. (A) Western blotting demonstrating expression levels of *Smad4*, synaptopodin and GAPDH in nephrin (+) cells isolated from *eNOS*^{-/-}PodCre ND, *eNOS*^{-/-}PodCre HFD+STZ, *eNOS*^{-/-}PodCre-*Smad4*^{-/-}ND and *eNOS*^{-/-}PodCre-*Smad4*^{-/-}HFD+STZ treated mouse kidneys. (B) Quantification of p57⁺ cells per Glomerular Cross Section (GCS) in *eNOS*^{-/-}PodCre ND, *eNOS*^{-/-}PodCre HFD+STZ, *eNOS*^{-/-}PodCre-*Smad4*^{-/-}ND and *eNOS*^{-/-}PodCre-*Smad4*^{-/-}HFD+STZ treated mouse kidneys. (C) Western blotting demonstrating expression levels of nephrin and α -Tubulin in *eNOS*^{-/-}PodCre ND, *eNOS*^{-/-}PodCre HFD+STZ, *eNOS*^{-/-}PodCre-*Smad4*^{-/-}ND and *eNOS*^{-/-}PodCre-*Smad4*^{-/-}HFD+STZ treated mouse kidneys. (D) Quantification of ratios of nephrin/ α -Tubulin in western blotting. (E) Periodic acid–Schiff (PAS) staining of sections from ND-treated or HFD+STZ-treated *eNOS*^{-/-}PodCre or *eNOS*^{-/-}PodCre-*Smad4*^{-/-} mouse kidneys. (F) Confocal microscopy demonstrated collagen IV expression in ND-treated or HFD+STZ-treated *eNOS*^{-/-}PodCre or *eNOS*^{-/-}PodCre-*Smad4*^{-/-} mouse kidneys. Quantitation of collagen IV staining area/glomerular cross-section (G), serum Cystatin C levels (H) and urinary albumin/creatinine ratio (I) in ND-treated or HFD+STZ-treated *eNOS*^{-/-}PodCre mouse or *eNOS*^{-/-}PodCre-*Smad4*^{-/-} mouse kidneys. Data are mean \pm s.d. from groups of eight mice. **P*<0.05, ***P*<0.01, ****P*<0.001.

Fig. 4

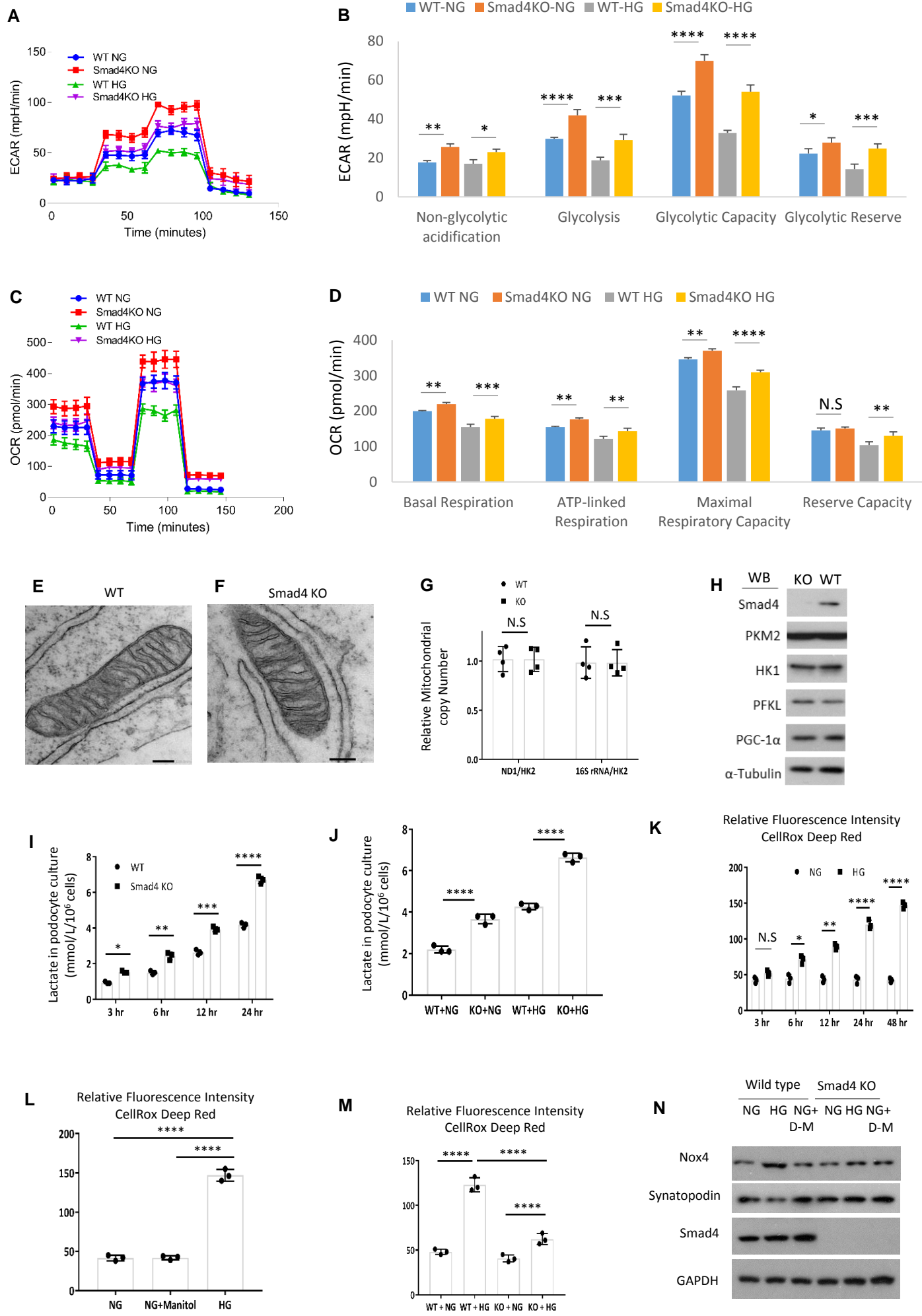


Figure 4. *Smad4* deficiency increases glycolysis and lactate production, decreases reactive oxygen species and protects podocytes from high glucose-induced injury. Wild type (WT) and *Smad4* KO mouse podocytes were treated with normal glucose (NG, 1g/L D-glucose) or high glucose (HG, 4.5g/L D-glucose) for 24 hrs then Seahorse was performed. Seahorse demonstrated real-time changes of ECAR in WT and *Smad4* KO podocytes after treatment with glucose, oligomycin and 2-Deoxy-D-glucose (2-DG) (A). Quantification of non-glycolytic acidification, glycolysis, glycolytic capacity and glycolytic reserve (B). Seahorse demonstrated real-time changes of oxygen consumption rate (OCR) after treatment with oligomycin, FCCP and rotenone in WT and *Smad4* KO podocytes (C). Quantification of basal, maximal, ATP-linked respiration and reserve capacity (D). All values are means \pm SD of at least three independent experiments. N.S, Not Significant, $P > 0.05$; * $P < 0.05$; ** $P < 0.01$; *** $P < 0.001$; **** $P < 0.0001$. Electron Microscopy demonstrated mitochondria morphology in WT (E) and *Smad4* KO (F) podocytes. (G) PCR demonstrated relative mitochondrial copy number in WT and *Smad4* KO podocytes. (H) Western blotting demonstrated expression of *Smad4*, HK1, PKM2, FPKL, PGC-1 α and α -tubulin in WT and *Smad4* KO podocytes. Lactate production in WT or *Smad4* KO podocytes under high glucose (HG) and normal glucose (NG) conditions (I, J). Relative fluorescence intensities of reactive oxygen species (ROS) under normal glucose (NG) or high glucose (HG) condition in podocytes (K). Relative fluorescence intensities of ROS after 24-hour NG, HG or NG+ D-manitol treatment in podocytes (L). Relative fluorescence intensities of ROS after 24-hour NG or HG treatment in WT or *Smad4* KO podocytes (M). Western blotting demonstrated NOX4 and synaptopodin expression after 24-hour NG or HG treatment in WT or *Smad4* KO podocytes (N). All values are means \pm SD of at least three independent experiments. * $P < 0.05$, ** $P < 0.01$, *** $P < 0.001$, **** $P < 0.0001$.

Fig 5

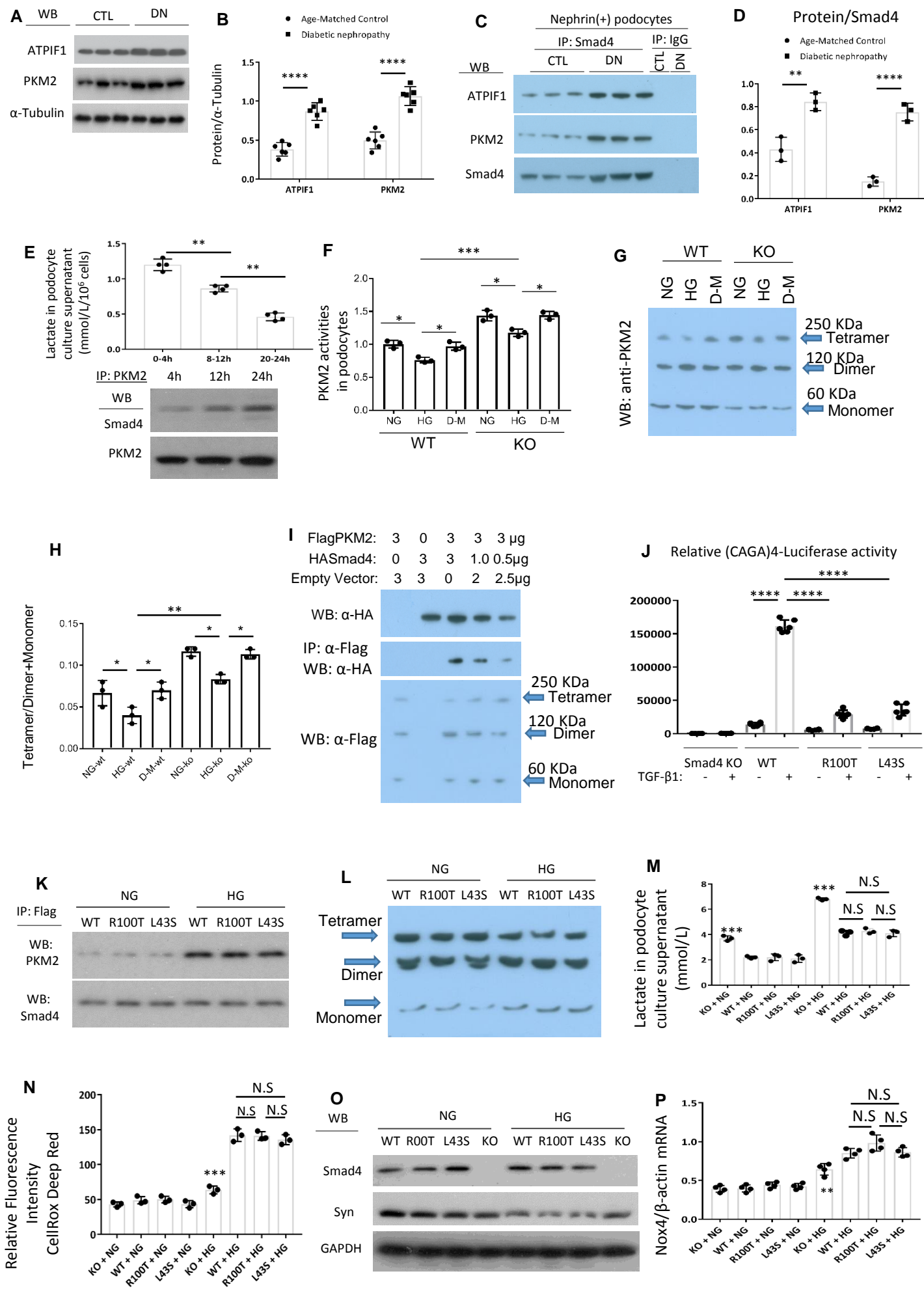
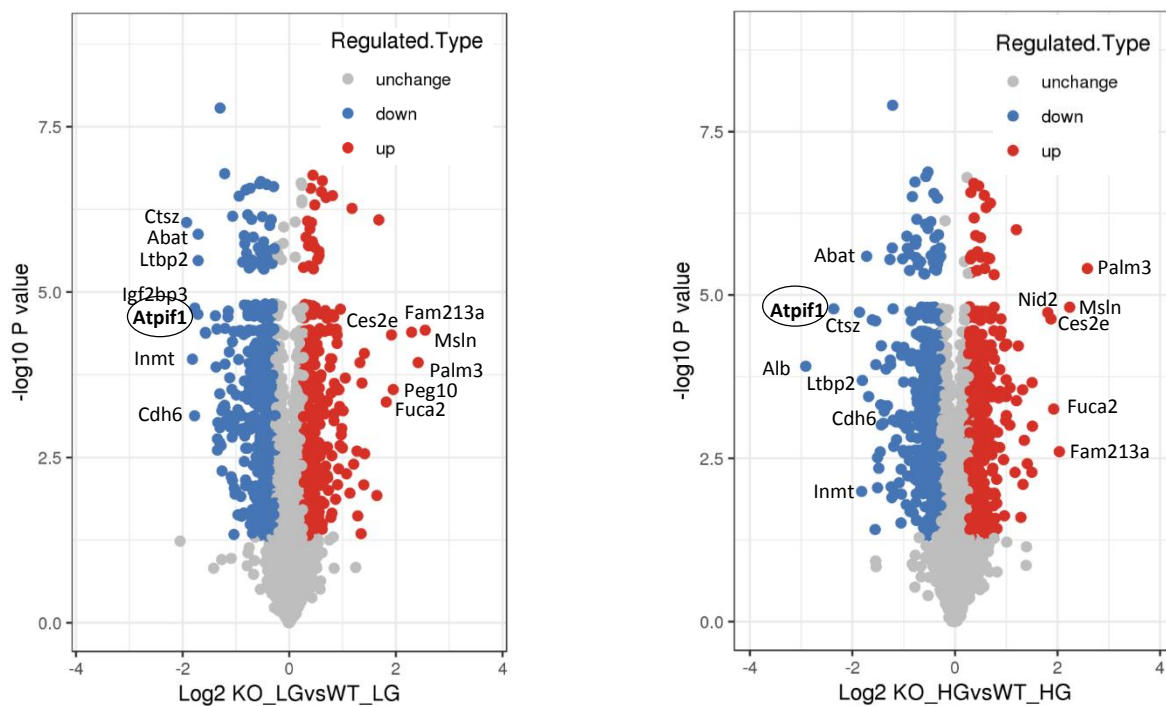


Figure 5. *Smad4* interacts with rate-limiting glycolytic enzyme PKM2 to modulate PKM2 tetramer formation and regulate lactate production in podocytes. WB demonstrated expression levels of ATPIF1 and PKM2 in age-matched kidneys and 16-week type 2 diabetic nephropathy (A). Quantitation of arbitrary ratios of ATPIF1 and PKM2 to α -Tubulin (B). Immunoprecipitation (IP)/WB demonstrated the interactions between *Smad4* and ATPIF1 and PKM2 in nephrin⁺ podocytes isolated from age-matched kidneys and 16-week type 2 diabetic nephropathy (C). Quantitation of arbitrary ratios of ATPIF1 and PKM2 to *Smad4* (D). Lactate production in different periods of under high glucose treatment in podocytes (upper panel), IP/WB demonstrated interaction between *Smad4* and PKM2 after 4-, 12- and 24-hour HG treatment in podocytes (lower panel) (E). PKM2 activities in wild type (WT), *Smad4* KO (KO) mouse podocytes under normal glucose (NG), high glucose (HG) or D-manitol (D-M) treatment for 24 hours (F). Western blotting demonstrated PKM2 tetramer, dimer and monomer after normal glucose (NG), high glucose (HG) or D-manitol (D-M) treatment for 24 hours in wild type (WT) or *Smad4* KO (KO) mouse podocytes after cross-linking treatment (G). Quantification of ratios of Tetramer/Dimer+Monomer. * $P < 0.05$; ** $P < 0.01$ (H). 293T cells were transduced with FlagPKM2, HAS*Smad4* and empty vector with various dosages. After 48 hours, cells were collected for Western blotting (upper panel), Immunoprecipitation/Western blotting (middle panel) and cross-linking/Western blotting (lower panel). Western blotting demonstrated expression levels of HA-*Smad4* (upper panel), interactions of FlagPKM2 with HAS*Smad4* (middle panel) and FlagPKM2 tetramer, dimer and monomer (lower panel) (I). *Smad4* KO podocytes were transduced with an empty retroviral vector, or retroviral vectors over-expressing *Smad4* WT, *Smad4* R100T, or *Smad4* L43S. SBE4-Luciferase assay demonstrated transcription activities in *Smad4* KO, *Smad4* WT, *Smad4* R100T and *Smad4* L43S podocytes with or without TGF- β 1 treatment (J). IP/WB demonstrated interaction between *Smad4* and PKM2 after 24-hour NG or HG treatment in WT, R100T and L43S podocytes (K). Cross-linking/Western blotting demonstrated PKM2 tetramer, dimer and monomer after 24-hour NG or HG treatment in WT, R100T and L43S podocytes (L). Lactate production in WT, R100T, L43S and *Smad4* KO podocytes after 24-hour NG or HG treatment (M). CellRox Deep Red test demonstrated relative fluorescence intensity in WT, R100T, L43S and *Smad4* KO podocytes treated with NG or HG for 24 hrs (N). WB demonstrated expression levels of Synaptopodin, *Smad4* and GAPDH in WT, R100T, L43S and *Smad4* KO podocytes treated with NG or HG for 24 hrs (O). RT-qPCR demonstrated ratios of Nox4/ β -actin in WT, R100T, L43S and *Smad4* KO podocytes treated with NG or HG for 24 hrs (P). One-way ANOVA, all values are means \pm SD of at least three independent experiments. ** $P < 0.01$; **** $P < 0.0001$; * $P < 0.05$ vs WT or vs R100T or L43S under HG condition; **** $P < 0.0001$ vs WT or vs R100T or L43S under NG or HG condition. N.S, not significant, $P > 0.05$.

Fig. 6

A



B

GO Terms Level 1	GO Terms Level 2	KO_HGvsKO_LG	KO_HGvsWT_HG	KO_LGvsWT_LG	WT_HGvsWT_LG	Identified
Biological Process	cellular process	206	1028	865	360	4739
	single-organism process	172	869	746	269	3807
	metabolic process	152	713	596	268	3424
Molecular Function	binding	220	1060	885	396	4795
	catalytic activity	115	480	417	154	2197
Cellular Component	cell	227	1173	997	414	5444
	organelle	212	1128	954	398	5102

C

Protein accession	Gene name	KO_LG/WT_LG		KO_HG/WT_HG		WT_HG/WT_LG		KO_HG/KO_LG	
		Ratio	P value						
P17710	HK1	1.132	0.146145	1.382	0.011656	1.063	0.51104	1.297	0.010324
O08528	HK2	1.167	0.178641	1.422	0.024519	0.994	0.93772	1.211	0.002585
P47857	PFKM	1.104	0.33708	0.96	0.51082	0.933	0.35664	0.811	0.106858
P52480	PKM	0.975	0.093361	0.896	0.001405	0.828	0.000104	0.761	3.65E-05
O35143	Atpif1	0.305	2.16E-05	0.194	1.63E-05	1.125	0.118417	0.717	0.004639
P63030	Mpc1	0.803	0.004744	0.699	0.004877	1.151	0.01018	1.002	0.96006
Q9CXZ1	Ndufs4	0.694	0.000136	0.678	0.000424	0.939	0.090362	0.918	0.062705
Q9DCS9	Ndufb10	0.762	0.001681	0.774	0.000182	0.952	0.021395	0.967	0.444
Q9D855	Uqcrb	0.676	0.002524	0.687	0.003916	0.89	0.030377	0.904	0.26296
Q61387	Cox7a2l	0.673	0.000323	0.678	0.002019	1.053	0.087402	1.061	0.024962

Fig 6. *Quantitative proteomic profiling for wild type (WT) and Smad4 knockout (KO) mouse podocytes under normal glucose (NG) or high glucose (HG) treatment. (A) Volcano plot of the protein abundance changes in response to NG or HG in WT or Smad4 KO podocytes. Average protein expression ratio of 3 replicates (log 2 transformed) between KO+NG vs WT+NG and KO+HG vs WT+HG. Different treatment groups were plotted against p-value by t-test ($-\log_{10}$ transformed). Cutoff of $p=0.05$ and 1.3-fold change were marked by blue and red dots, respectively. (B) Functional annotation of altered proteome in four experimental groups. A GO analysis of the significantly changed proteins identified in proteomic analysis for biological process, molecular function, and KEGG pathway. (C) The figure shows protein access number, gene name, ratio and p value in four experiment groups in quantitative Mass Spectrometry.*

Fig. 7

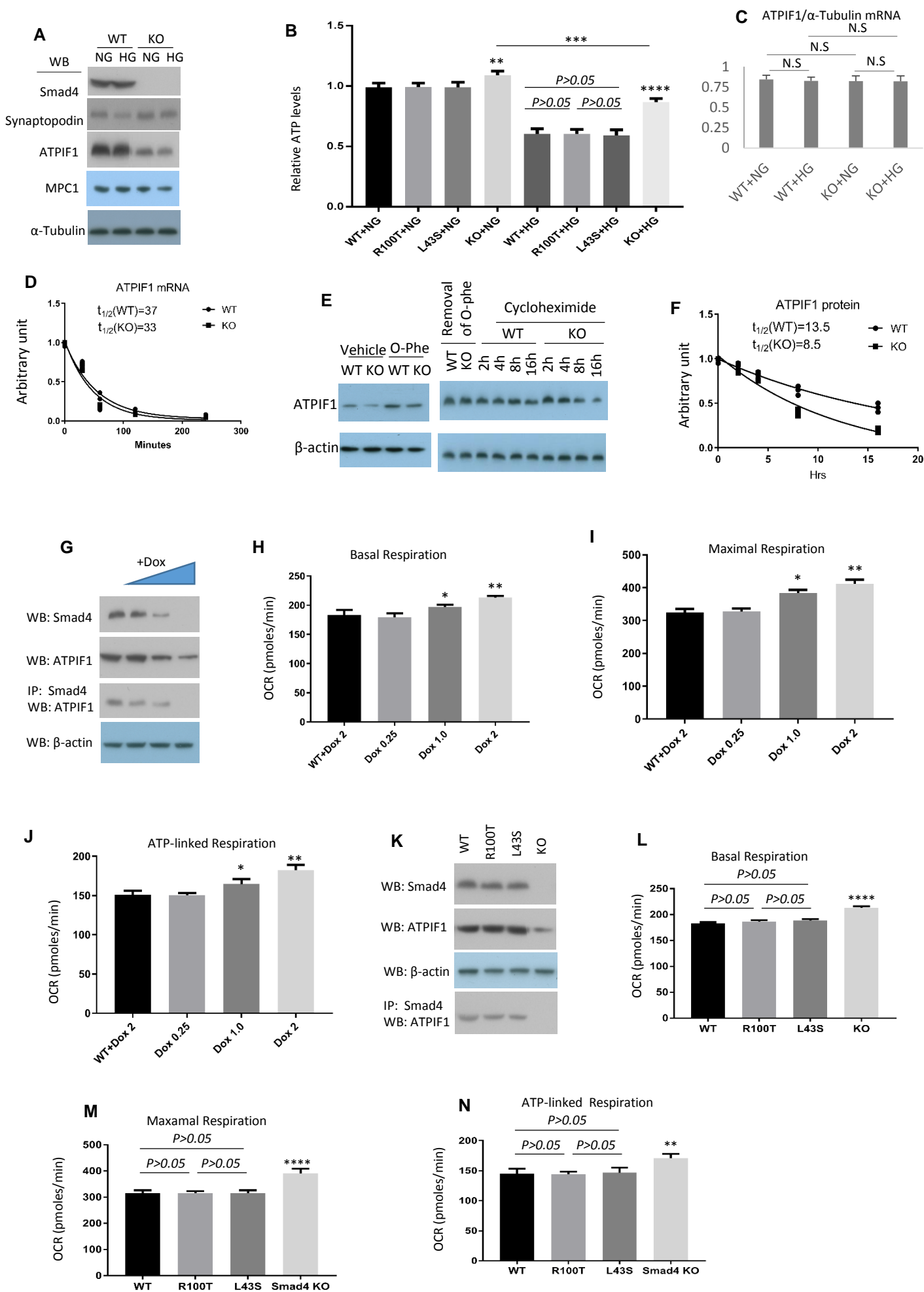
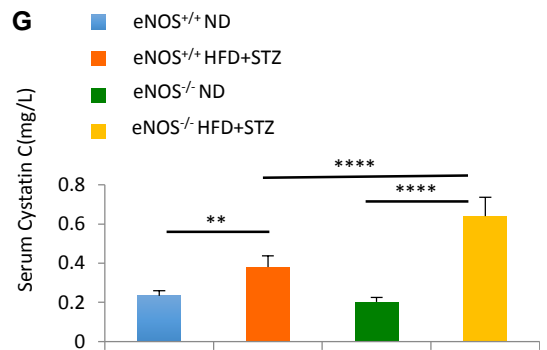
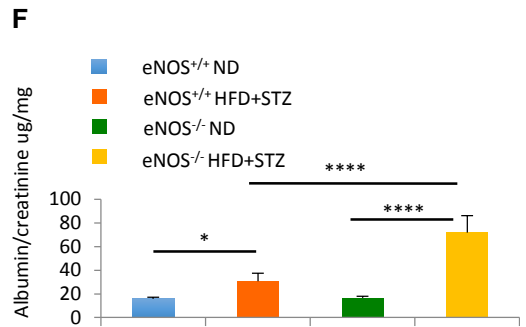
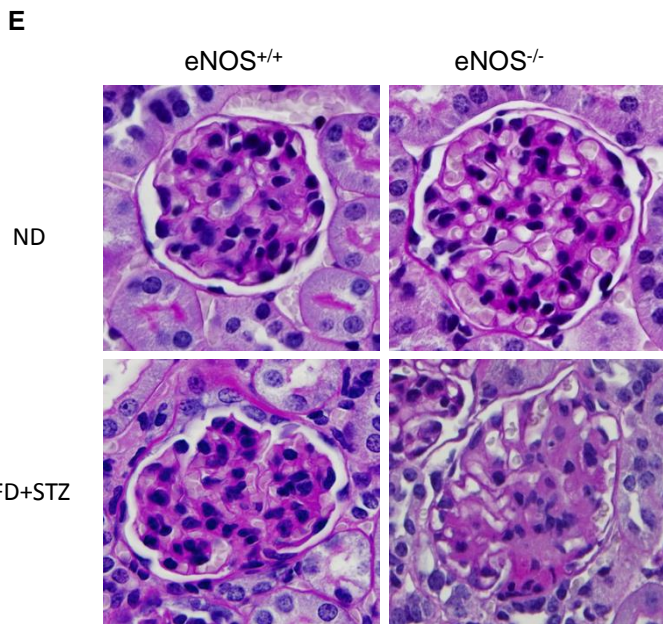
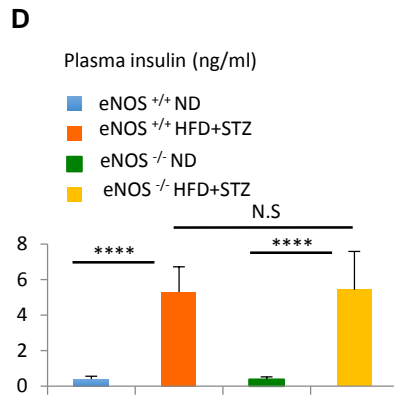
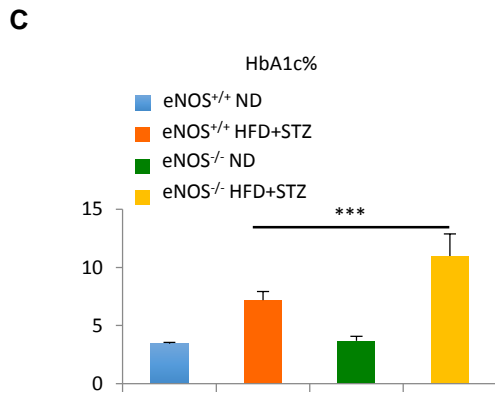
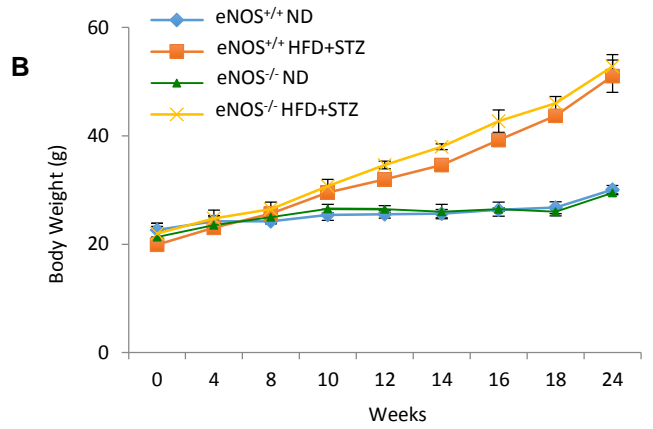
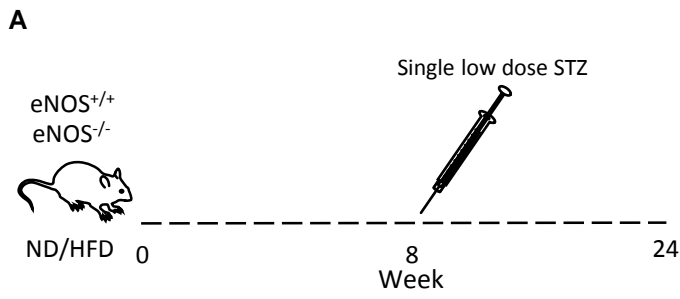


Figure 7. *Smad4* interacts with *ATPIF1* to regulate the activity of mitochondrial oxidative

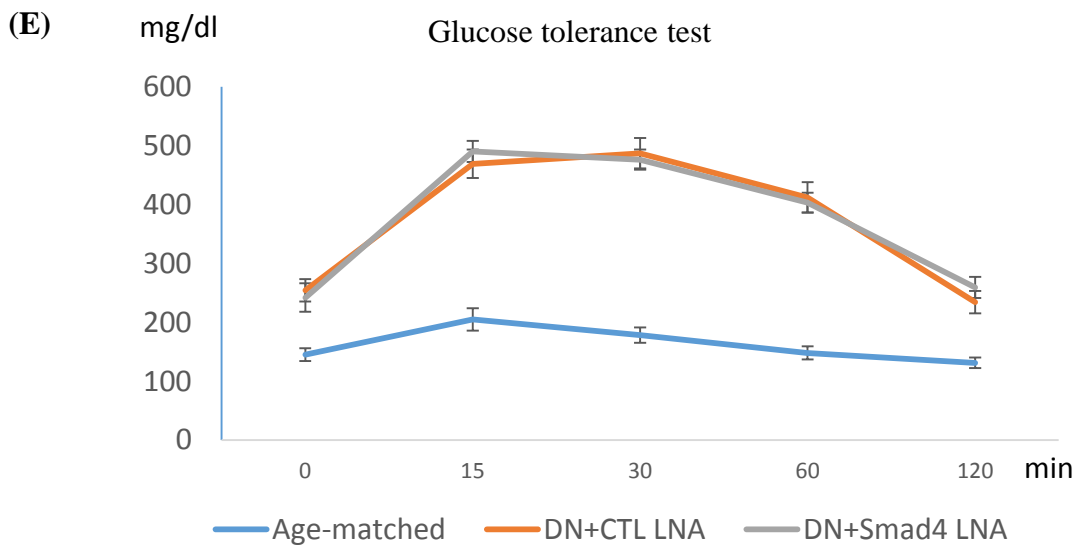
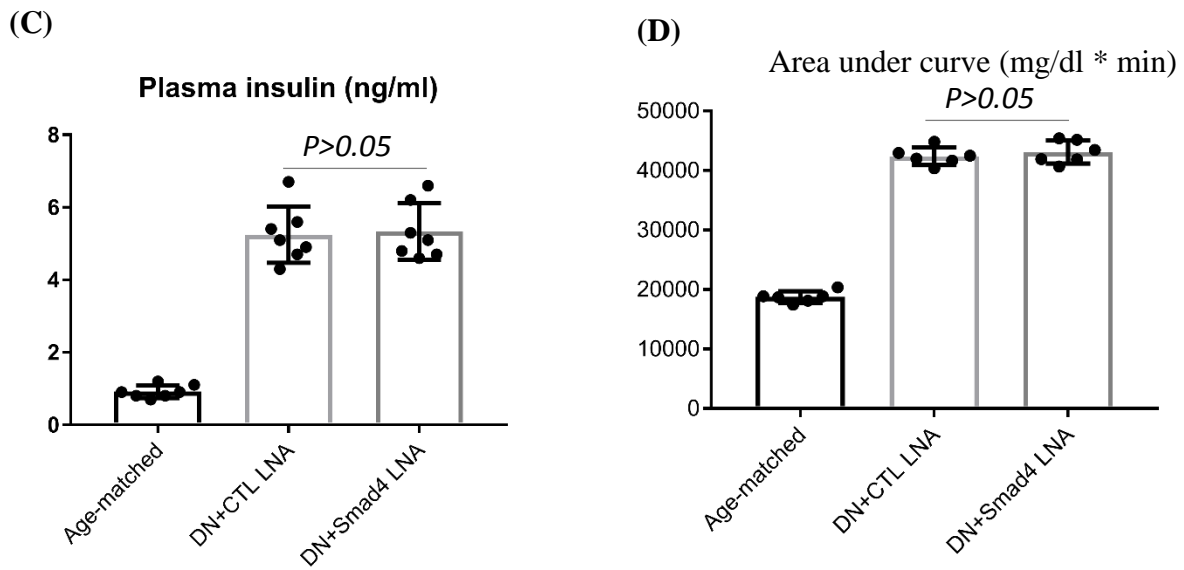
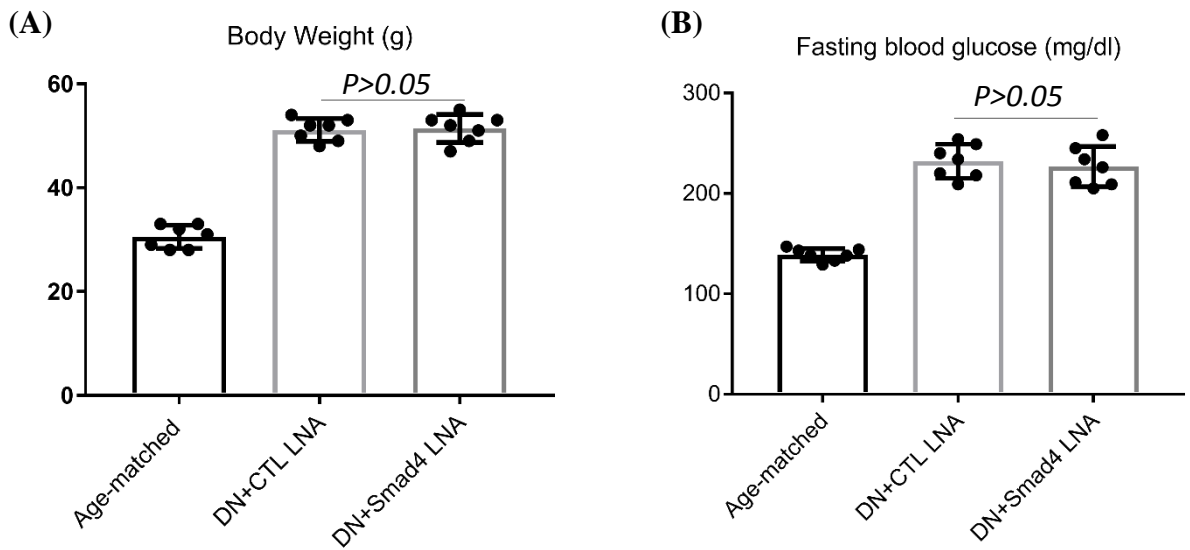
phosphorylation in mouse podocytes. (A) Western blotting (WB) demonstrated the expression levels of *Smad4*, *Synaptopodin*, *ATPIF1*, *MPC1* and α -*Tubulin* in *Smad4* deficient and wild type mouse podocytes under normal glucose (1g/L D-glucose, NG) or high glucose (4.5g/L D-glucose HG) condition. (B) Relative ATP levels in *Smad4* WT, *Smad4* R100T, *Smad4* L43S or *Smad4* KO podocytes treated with NG or HG for 24 hours. All values are means \pm SD of at least three independent experiments. * $P < 0.05$, ** $P < 0.01$, *** $P < 0.001$. N.S, $P > 0.05$. (C) RT-qPCR demonstrated relative mRNA levels of *ATPIF1* in WT or *Smad4* KO mouse podocytes treated with NG or HG for 24hrs. (D) Decay curves demonstrated *ATPIF1* mRNA half-life 30, 60, 120 and 140 mins after wild type (WT) or *Smad4* knockout (KO) mouse podocyte were treated with 5 μ g/ml actinomycin D. (E) Western blotting demonstrated *ATPIF1* expression levels in wild type or *Smad4* KO mouse podocytes after treatment with 0.5 mM *o*-phe for 1hr, or treatment with *o*-phe then removal of *o*-phe and treatment with 20 μ g/ml cycloheximide for different periods of time as indicated. (F) Decay curves demonstrated *ATPIF1* protein half-life after wild type (WT) or *Smad4* knockout (KO) mouse podocyte were treated with 0.5 mM *o*-phenanthroline (*o*-phe) for 1 hr then *o*-phe was replaced with 20 μ g/ml cycloheximide for different periods of time. (G) Doxycycline (Dox) inducible sgRNA cassette/cas9 system to delete *Smad4* gene was employed in mouse podocytes. WB and IP/WB demonstrated that expression of *Smad4* and *ATPIF1* and the interaction between *Smad4* and *ATPIF1* decrease following Dox treatment. Seahorse demonstrated oxygen consumption rate (OCR) in Basal (H), Maximal (I) and ATP-linked Respiration (J) in WT or Dox-inducible sgRNA cassette/cas9 system in podocytes treated with different dosages of Dox. (K-N) *Smad4* KO podocytes were transduced with an empty retroviral vector, or retroviral vectors over-expressing *Smad4* WT, *Smad4* R100T, or *Smad4* L43S. Western blotting demonstrated expression levels of *Smad4*, *ATPIF1* and β -actin (K). IP/WB demonstrated interaction between *Smad4* and *ATPIF1* in *Smad4* WT, *Smad4* R100T, and *Smad4* L43S podocytes (K). Seahorse demonstrated OCR in Basal (L), Maximal (M) and ATP-linked Respiration (N) in *Smad4* WT, *Smad4* R100T, *Smad4* L43S or *Smad4* KO podocytes. All values are means \pm SD of at least three independent experiments. * $P < 0.05$, ** $P < 0.01$, *** $P < 0.001$. N.S, $P > 0.05$.

Supp Fig 1



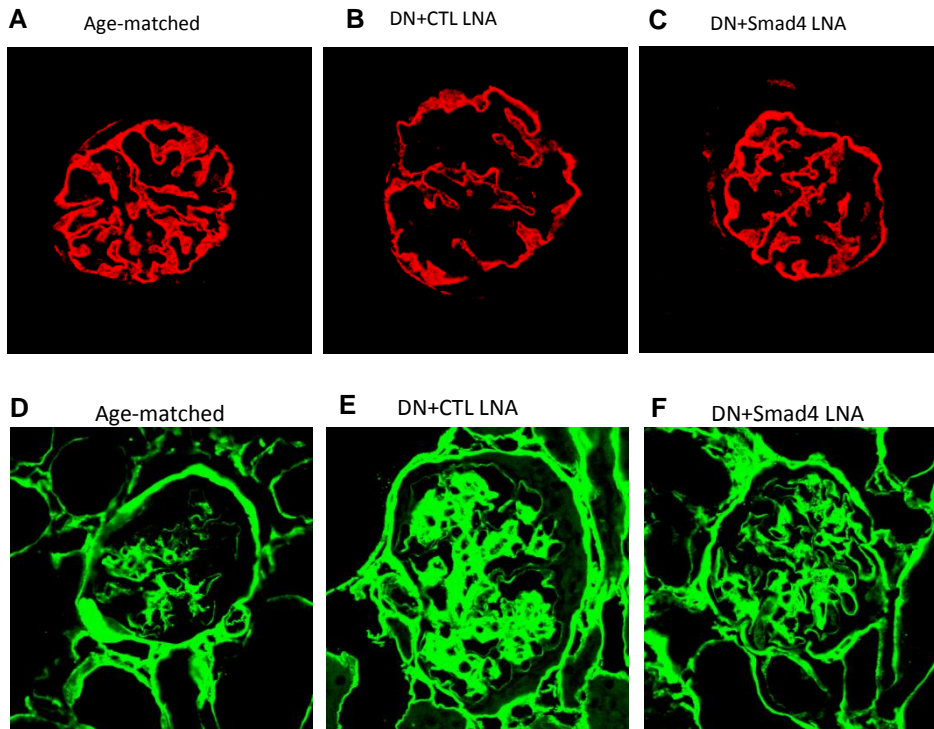
Suppl. Fig 1. (A) Schema illustrating mouse model of type II diabetic nephropathy using high fat diet (HFD) and a single dose streptozotocin (50mg/Kg) intraperitoneal injection. (B) Increment change of body weight in *eNOS*^{+/+} ND, *eNOS*^{+/+} HFD+STZ, *eNOS*^{-/-}ND and *eNOS*^{-/-} HFD+STZ. (C, D) HbA1c% (C) and plasma insulin level (D) change in *eNOS*^{+/+} ND, *eNOS*^{+/+} HFD+STZ, *eNOS*^{-/-}ND and *eNOS*^{-/-} HFD+STZ after 24 weeks of treatment. (E) Periodic acid–Schiff (PAS) staining of sections from *eNOS*^{+/+} ND, *eNOS*^{+/+} HFD+STZ, *eNOS*^{-/-}ND and *eNOS*^{-/-} HFD+STZ mouse kidneys. (F) Urinary albumin/creatinine ratio changes from *eNOS*^{+/+} ND, *eNOS*^{+/+} HFD+STZ, *eNOS*^{-/-}ND and *eNOS*^{-/-} HFD+STZ mouse. (G) Serum cystatin C changes from *eNOS*^{+/+} ND, *eNOS*^{+/+} HFD+STZ, *eNOS*^{-/-}ND and *eNOS*^{-/-} HFD+STZ mouse. Data are mean \pm s.d. from groups of eight mice. **P*<0.05, ***P*<0.01, ****P*<0.001.

Supp Fig 2



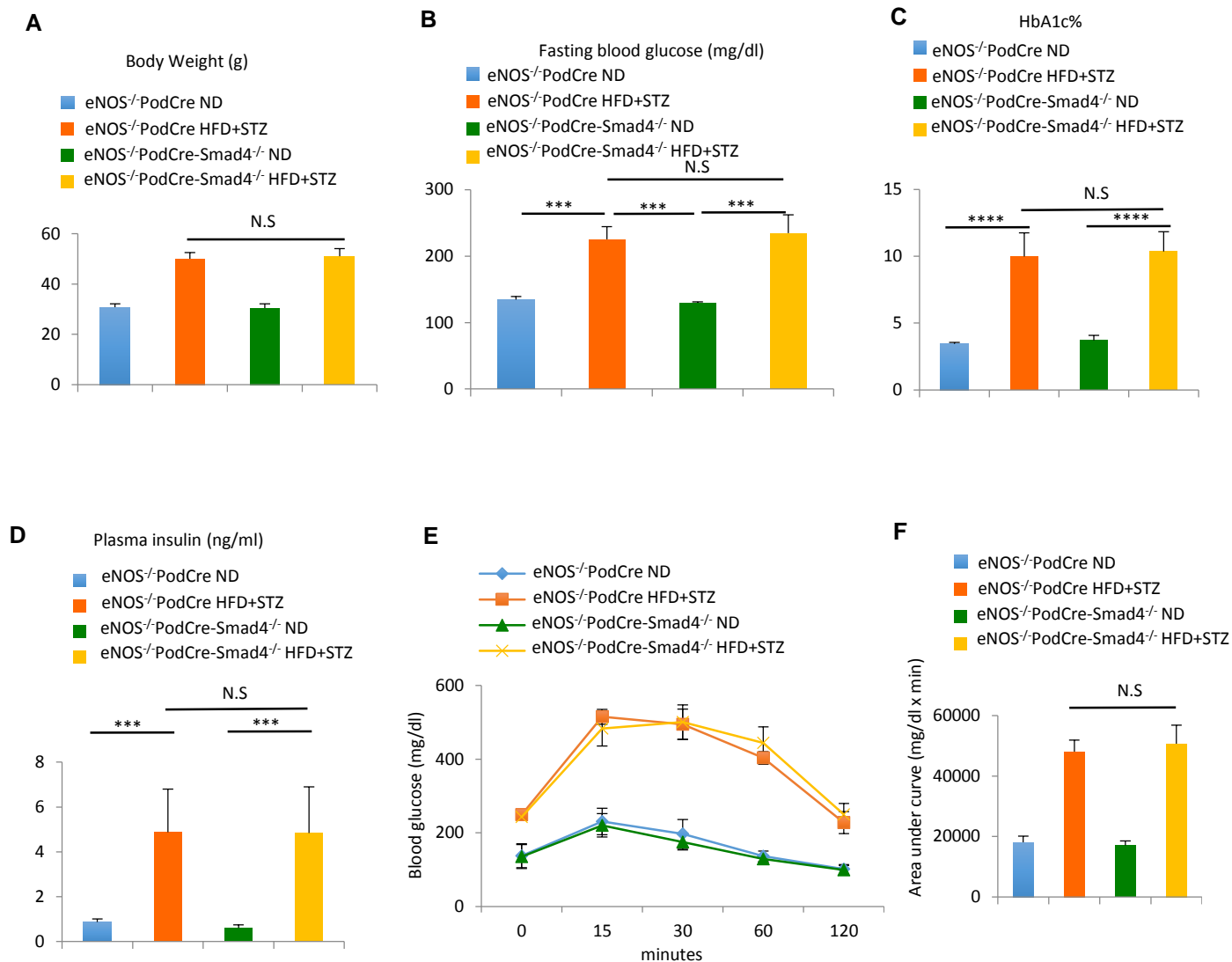
Suppl. Fig 2. *Smad4* LNA administration retards the progression of mouse type 2 diabetic nephropathy. (A-C) changes in body weight, fasting blood glucose levels, and plasma insulin in age-matched, control-LNA (CTL-LNA)-treated or *Smad4* LNA-treated in type 2 diabetic *eNOS*^{-/-} mice. Glucose tolerance test (E) and quantification of Glucose tolerance test (D) in age-matched, control-LNA (CTL-LNA)-treated or *Smad4* LNA-treated in type 2 diabetic *eNOS*^{-/-} mice. Data are mean \pm s.d. from groups of 6 mice. One way ANOVA.

Suppl Fig 3

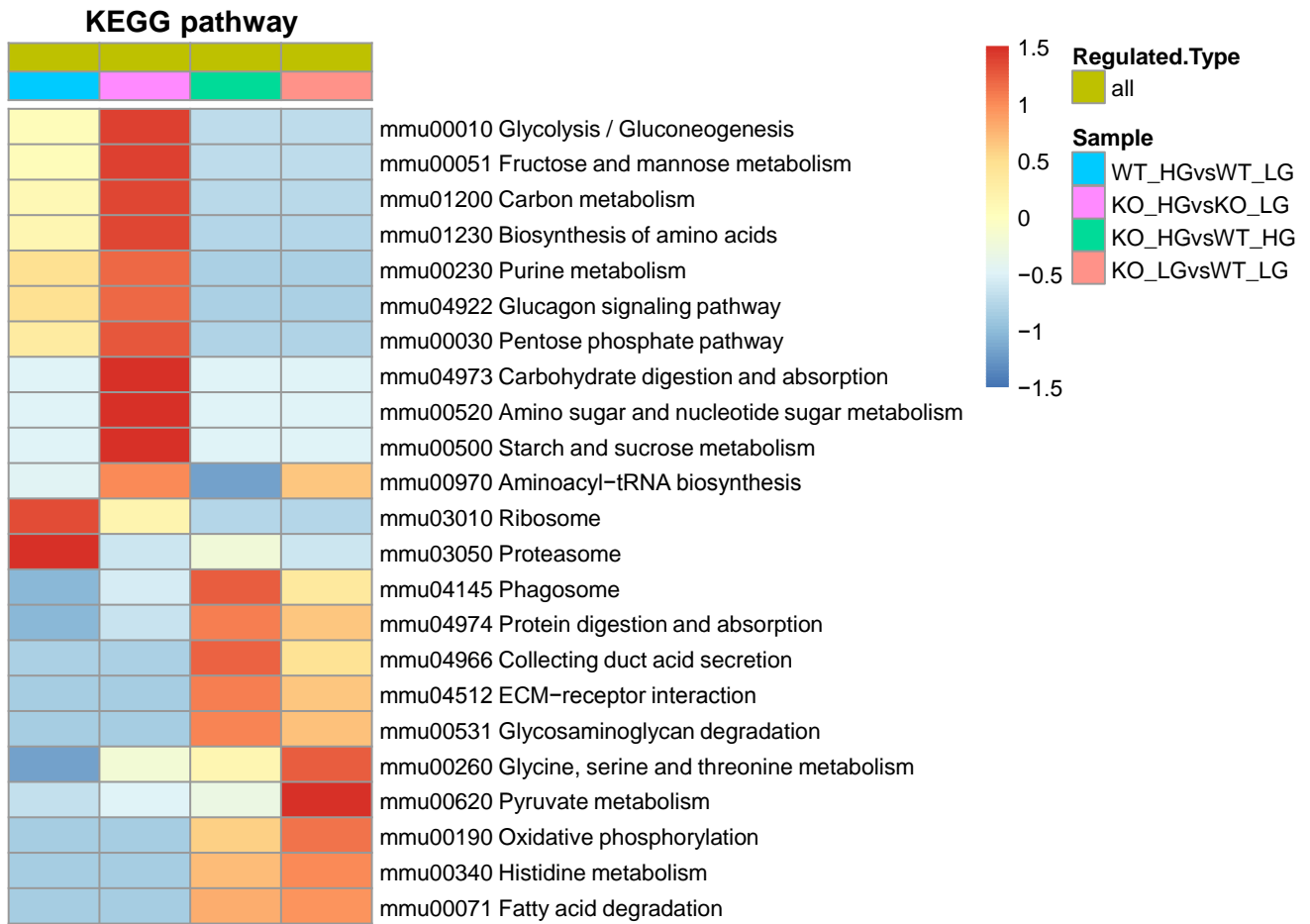


Suppl. Fig 3. Smad4 LNA treatment decreases podocyte injury and glomerulosclerosis in type 2 diabetic nephropathy. Confocal microscopy demonstrated synaptopodin (red, A-C) collagen IV expression (green, D-F) in age-matched kidney, CTL LNA treated diabetic nephropathy and Smad4 LNA-treated diabetic nephropathy.

Suppl Fig 4



Suppl. Fig 4. *Smad4* deficiency in podocytes protects mice from type 2 diabetic nephropathy. (A-D) changes in body weight, fasting blood glucose levels, HbA1c and plasma insulin in ND-treated or HFD+STZ-treated eNOS^{-/-}PodCre mice or eNOS^{-/-}PodCre-Smad4^{-/-} mice. Glucose tolerance test (E) and quantification of Glucose tolerance test (F) in ND-treated or HFD+STZ-treated eNOS^{-/-}PodCre mice or eNOS^{-/-}PodCre-Smad4^{-/-} mice. Data are mean \pm s.d. from groups of eight mice. N.S, $P > 0.05$; * $P < 0.05$; ** $P < 0.01$; *** $P < 0.001$.



Suppl Fig 5. Encyclopedia of Genes and Genomes (KEGG) database annotates protein pathways in wild type or *Smad4* deficient podocytes treated with normal glucose or high glucose.